U-Pb zircon geochronology and depositional age models for the Upper Triassic Chinle Formation (Petrified Forest National Park, Arizona, USA): Implications for Late Triassic paleoecological and paleoenvironmental change

Cornelia Rasmussen[1,2,3,†], Roland Mundil[4], Randall B. Irmis[1,2], Dominique Geisler[5], George E. Gehrels[5], Paul E. Olsen[6], Dennis V. Kent[6,7], Christopher Lepre[6,7], Sean T. Kinney[6], John W. Geissman[8,9], and William G. Parker[10]

[1]*Department of Geology & Geophysics, University of Utah, Salt Lake City, Utah 84112-0102, USA*
[2]*Natural History Museum of Utah, University of Utah, Salt Lake City, Utah 84108-1214, USA*
[3]*Institute for Geophysics, Jackson School of Geosciences, University of Texas at Austin, Austin, Texas 78758, USA*
[4]*Berkeley Geochronology Center, Berkeley, California 94709, USA*
[5]*Department of Geosciences, University of Arizona, Tucson, Arizona 85721, USA*
[6]*Lamont-Doherty Earth Observatory, Columbia University, Palisades, New York 10964, USA*
[7]*Department of Earth and Planetary Sciences, Rutgers University, Piscataway, New Jersey 08854, USA*
[8]*Department of Geosciences, University of Texas at Dallas, Richardson, Texas 75080, USA*
[9]*Department of Earth and Planetary Sciences, University of New Mexico, Albuquerque, New Mexico, 87131-0001, USA*
[10]*Division of Science and Resource Management, Petrified Forest National Park, Petrified Forest, Arizona 86028, USA*

ABSTRACT

The Upper Triassic Chinle Formation is a critical non-marine archive of low-paleolatitude biotic and environmental change in southwestern North America. The well-studied and highly fossiliferous Chinle strata at Petrified Forest National Park (PFNP), Arizona, preserve a biotic turnover event recorded by vertebrate and palynomorph fossils, which has been alternatively hypothesized to coincide with tectonically driven climate change or with the Manicouagan impact event at ca. 215.5 Ma. Previous outcrop-based geochronologic age constraints are difficult to put in an accurate stratigraphic framework because lateral facies changes and discontinuous outcrops allow for multiple interpretations. A major goal of the Colorado Plateau Coring Project (CPCP) was to retrieve a continuous record in unambiguous superposition designed to remedy this situation. We sampled the 520-m-long core 1A of the CPCP to develop an accurate age model in unquestionable superposition by combining U-Pb zircon ages and magnetostratigraphy. From 13 horizons of volcanic detritus-rich siltstone and sandstone, we screened up to ~300 zircon crystals per sample using laser ablation–inductively coupled plasma–mass spectrometry and subsequently analyzed up to 19 crystals of the youngest age population using the chemical abrasion–isotope dilution–thermal ionization mass (CA-ID-TIMS) spectrometry method. These data provide new maximum depositional ages for the top of the Moenkopi Formation (ca. 241 Ma), the lower Blue Mesa Member (ca. 222 Ma), and the lower (ca. 218 to 217 Ma) and upper (ca. 213.5 Ma) Sonsela Member. The maximum depositional ages obtained for the upper Chinle Formation fall well within previously proposed age constraints, whereas the maximum depositional ages for the lower Chinle Formation are relatively younger than previously proposed ages from outcrop; however, core to outcrop stratigraphic correlations remain uncertain. By correlating our new ages with the magnetostratigraphy of the core, two feasible age model solutions can be proposed. Model 1 assumes that the youngest, coherent U-Pb age clusters of each sample are representative of the maximum depositional ages and are close to the true time of deposition throughout the Sonsela Member. This model suggests a significant decrease in average sediment accumulation rate in the mid-Sonsela Member. Hence, the biotic turnover preserved in the mid-Sonsela Member at PFNP is also middle Norian in age, but may, at least partially, be an artifact of a condensed section. Model 2 following the magnetostratigraphic-based age model for the CPCP core 1A suggests instead that the ages from the lower and middle Sonsela Member are inherited populations of zircon crystals that are 1–3 Ma older than the true depositional age of the strata. This results in a model in which no sudden decrease in sediment accumulation rate is necessary and implies that the base of the Sonsela Member is no older than ca. 216 Ma. Independent of these alternatives, both age models agree that none of the preserved Chinle Formation in PFNP is Carnian (>227 Ma) in age, and hence the biotic turnover event cannot be correlated to the Carnian–Norian boundary but is rather a mid-Norian event. Our age models demonstrate the powers, but also the challenges, of integrating detrital CA-ID-TIMS ages with magnetostratigraphic data to properly interpret complex sedimentary sequences.

Cornelia Rasmussen ⓘ http://orcid.org/0000-0001-9979-8224

†crasmussen@utexas.edu.

INTRODUCTION

The Triassic Period represents a critical time in Earth history that experienced major environmental changes, and is embedded between two mass extinction events (e.g., Payne et al., 2004; Mundil et al., 2004; Irmis and Whiteside, 2010; Preto et al., 2010; Schoene et al., 2010). Key Triassic Earth system events include the onset of the break up and northward drift of the supercontinent Pangea (Dietz and Holden, 1970; Robinson, 1973; Olsen, 1997; Olsen and Kent, 2000), frequent carbon cycle excursions, and major changes in pCO$_2$ levels (e.g., Payne et al., 2004; Berner, 2006; Whiteside et al., 2010; Hönisch et al., 2012; Schaller et al., 2015; Foster et al., 2017). During the Late Triassic, sudden paleoenvironmental events include reoccurring flood basalt volcanism such as the Wrangellia Large Igneous Province (Greene et al., 2010, and references within) and the Central Atlantic Magmatic Province (Whiteside et al., 2010; Schoene et al., 2010; Blackburn et al., 2013), as well as at least three hypervelocity impact events, the largest of which is the Manicouagan impact structure in Canada (Ramezani et al., 2005; Grieve, 2006; Schmieder et al., 2010, 2014; Cohen et al., 2017). At the same time, the Late Triassic witnessed a number of important evolutionary events, such as the origin and early diversification of dinosaurs, lizards, mammaliaforms, and lissamphibians on land, and the diversification of scleractinian corals and calcareous nannoplankton in the ocean (e.g., Rogers et al., 1993; Stanley, 2003; Falkowski et al., 2004; Furin et al., 2006; Luo, 2007; Irmis, 2011; Fraser and Sues, 2011; Stocker et al., 2019).

Previously published precise geochronologic ages for the Late Triassic are scarce (Furin et al., 2006; Mundil, 2007; Mundil et al., 2010) and have primarily focused on the Triassic–Jurassic boundary and end-Triassic extinction (e.g., Schaltegger et al., 2008; Schoene et al., 2010; Blackburn et al., 2013). This problem is particularly acute given that the Late Triassic represents two-thirds of the duration of the entire Triassic Period but has an order of magnitude fewer numerical ages than the Early to Middle Triassic (Mundil et al. 2010). Thus, the lack of Late Triassic ages hampers our ability to test first-order hypotheses about the correlation and duration of major evolutionary and paleoenvironmental events. Precise and accurate radioisotopic ages are particularly critical in non-marine sequences, because geochronology is a direct means to link these records to the marine-defined Global Boundary Stratotype Section and Point (GSSP)-based timescale or to provide anchor ages for magnetostratigraphic correlation, and also because lateral facies changes complicate lithostratigraphic correlations even over short distances (e.g., Parker and Martz, 2010; Irmis et al., 2011; Ramezani et al., 2011; Atchley et al., 2013). Exemplifying these difficulties, some precise U-Pb ages are available for the intensely studied Upper Triassic Chinle Formation and its equivalents in western North America (Irmis et al., 2011; Ramezani et al., 2011, 2014; Atchley et al., 2013), yet these outcrop samples are spread over hundreds of square kilometers, so placing them into a single unambiguous superposition remains difficult despite excellent outcrop.

To date, the only comprehensive timescale for the Late Triassic has been the Newark–Hartford Astrochronostratigraphic Polarity Time Scale (N–H APTS) (Kent et al., 2017), which is calibrated by orbitally paced lacustrine cycles but has direct geochronologic control for only a ~600 k.y. window around the Triassic–Jurassic boundary (Blackburn et al., 2013). Though the Astrochronostratigraphic Polarity Time Scale (N–H APTS) has been incorporated into various time scale compilations (e.g., Ogg, 2012; Walker et al., 2018), until very recently (Kent et al., 2018; Olsen et al., 2019) there has been no direct tests of its validity.

The Chinle Formation exposed at Petrified Forest National Park (PFNP) in northern Arizona, USA, represents an ideal study area to resolve these issues for two reasons: first, the sedimentary strata contain a vast amount of volcanic detritus generally interpreted as introduced by the neighboring Cordilleran arc (e.g., Schultz, 1963; Stewart et al., 1986; Howell and Blakey, 2013) that allow, even if no primary volcanic deposits are present, the reconstruction of maximum depositional ages for these strata because they contain juvenile zircons that can be dated using the U-Pb method. In these cases, a sedimentary bed for which a maximum depositional age has been obtained must be the same age or younger than this U-Pb age (i.e., the youngest zircon crystals may have been redeposited over an unknown amount of time before final deposition). U-Pb dating of redeposited volcanic zircon crystals has already been validated using outcrop samples in PFNP and surrounding areas (Dickinson and Gehrels, 2009; Ramezani et al., 2011; Atchley et al., 2013) and other Chinle exposures (Irmis et al., 2011; Marsh et al., 2019). Second, the sedimentary strata contain a primary non-marine archive for the North American Late Triassic environments including a well-studied sedimentology and fossil record (including vertebrates, invertebrates, and palynomorphs) (e.g., Ash, 1980, 2005; Dubiel et al., 1991; Dubiel, 1994; Good, 1998; Irmis, 2005; Parker, 2005, 2006; Martz and Parker, 2010; Reichgelt et al., 2013).

Particularly of interest in the Chinle record is the possibility of recovering major Earth life events. For example, a biotic turnover in palynomorph (Reichgelt et al., 2013; Baranyi et al., 2018) and vertebrate taxa (Parker and Martz, 2010) occurs in outcrop in the middle Sonsela Member between 213.1 Ma and 218.0 Ma, based on outcrop correlation of dated horizons in Ramezani et al. (2011) and the biostratigraphic record (e.g., Parker and Martz, 2010). Three main hypotheses have been suggested as the potential cause for the biotic turnover: (1) increasing aridification driven by either northward drift of Pangaea or tectonic changes along the western margin of the North American Cordillera (Atchley et al., 2013; Lindström et al., 2016); (2) ecosystem disruption caused by the relatively large (crater diameter ~100 km) Manicouagan impact event in Quebec, Canada (e.g., Grieve, 2006) at ca. 215.5 Ma (Ramezani et al., 2005) (Mundil and Irmis, 2008; Olsen et al., 2010; Parker and Martz, 2010); and (3) partially an artifact of the stratigraphic record (for example due to one or more hiatuses), making a gradual biotic turnover appear sudden and coordinated due to a condensed section (Heckert and Lucas, 1996). Similarly, although recent geochronology suggests the fossil-bearing levels of the Chinle Formation are wholly Norian in age (Irmis et al., 2011; Ramezani et al., 2011, 2014), some authors maintain that the lower Chinle is Carnian in age (e.g., Lucas and Tanner, 2018) and preserves a record of the Carnian Pluvial Event known from the Tethys (e.g., Lucas and Tanner, 2018; Baranyi et al., 2019), a possibly global climate event prior to 230 Ma. Therefore, the Chinle Formation preserves a geologic record ideally suited to test hypotheses about biotic responses to paleoclimate change, hypervelocity impact events, and the northward movement of Pangea through different climate zones (cf. Kent and Tauxe, 2005; Whiteside et al., 2011).

Given the contentious and unresolved lithostratigraphic correlation of the Chinle Formation even within PFNP (see discussion in Martz and Parker, 2010), the Colorado Plateau Coring Project (CPCP) was established to obtain a continuous cored section in the park to provide unambiguous superposition for high-resolution magnetostratigraphic and radioisotopic sampling. In 2013, three cores (1A, 2A, and 2B) from the northern and the southern part of PFNP were recovered, respectively (Fig. 1; Olsen et al., 2018). By sampling throughout the Chinle Formation portion of core 1A, which covers nearly the entire section preserved in outcrop, we seek in this study to develop high-resolution age models, constrained by U-Pb ages and magnetostratigraphy (based on Kent et al., 2018, 2019), that can test the above hypotheses for the causes of Late Triassic biotic and paleoenvironmental
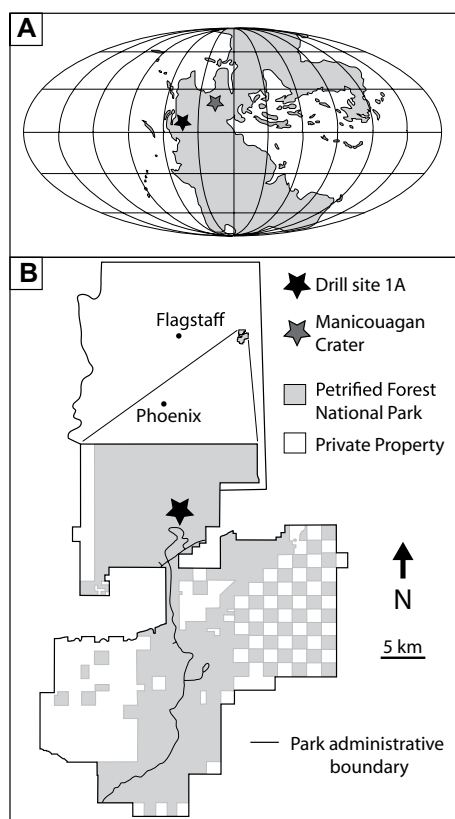
Figure 1. (A) Approximate location of Petrified Forest National Park (PFNP) and the Manicouagan impact site on the supercontinent Pangea (map after Blakey, 2008) and (B) map of PFNP in northern Arizona. The CPCP drill site 1A at the northern part of PFNP is marked by a black star (map after Parker and Martz, 2010).

events recorded in western North America. Initial results from the upper part of the core demonstrate the power of this approach and helped to confirm the stability of the 405 k.y. eccentricity cycle in geologic deep time, and thereby confirmed the accuracy of the N–H APTS (Kent et al., 2018; Olsen et al., 2019). New magnetostratigraphic results for the lower portion of core 1A are reported elsewhere (Kent et al., 2019) but are also discussed here in the context of the new U-Pb data.

GEOLOGIC SETTING

At PFNP, extensive exposures of the Upper Triassic Chinle Formation have been subject to a vast number of stratigraphic, sedimentologic, and paleontologic studies throughout the last century (e.g., Martz and Parker, 2010, and references therein). A concise stratigraphic unit description and detailed geologic map for Chinle Formation outcrops in the PFNP area is avail-

able in Martz et al. (2012), and we follow their stratigraphic nomenclature. Additional recent sedimentologic/stratigraphic summaries are available in Martz and Parker (2010), Atchley et al. (2013), Howell and Blakey (2013), Nordt et al. (2015), and Olsen et al. (2018).

Based on the leading interpretation, these Triassic sediments have been deposited in an actively subsiding backarc basin bordered toward the west by the Cordilleran arc system (Stewart et al., 1972a, 1972b; Dubiel et al., 1991; Howell and Blakey, 2013; Riggs et al., 2016). At this time, the basin was located close to the paleo-equator (5–15°N) (Kent and Tauxe, 2005; Kent and Irving, 2010) and was bordered toward the west by the Cordilleran arc system, which introduced vast amounts of volcanic detritus into the Chinle depocenter (Howell and Blakey, 2013; Riggs et al., 2012, 2016). Many authors recognized that the claystones and clay-bearing sandstones of the lower Chinle Formation contain a large amount of volcanic lithic detritus including tuff and other volcanic clasts as well as volcanically derived minerals such as sanidine, euhedral biotite, and plagioclase (e.g., Allen, 1930; Cadigan, 1963; Schultz, 1963; Stewart et al., 1986; Riggs et al., 1996). Stewart et al. (1986) report that up to three-quarters of the lower Chinle Formation consists of volcanic detritus that can be found within deposits of variable grain size, ranging from claystone to conglomerate beds, an observation also supported by more recent studies (e.g., Riggs et al., 2012, 2013, 2016). Thus, this makes the formation potentially ideal for developing maximum depositional ages from volcanic minerals such as zircon, even if discrete ash-fall horizons are obscure or absent.

The Chinle Formation is predominantly fluvial in origin, comprising a broad complex of floodplains and tributary streams draining into larger rivers flowing to the northwest toward the eastern margin of the Panthalassa Ocean (Stewart et al., 1972a, 1972b; Blakey and Gubitosa, 1983; Dubiel, 1994; Riggs et al., 1996; Dickinson and Gehrels, 2008a, 2008b). The depositional style of these fluvial systems varied considerably over the life of the Chinle deposystem, with large permanent meandering streams and poorly drained floodplains (e.g., oxisols, histosols, and alfisols) in the lower Chinle, transitioning into flashier, more seasonal flow with well-drained floodplains (e.g., vertisols, calcisols, and aridisols) in the upper part of the formation (Blakey and Gubitosa, 1983, 1984; Dubiel et al., 1991; Dubiel, 1994; Dubiel and Hasiotis, 2011; Trendell et al., 2012, 2013; Atchley et al., 2013; Howell and Blakey, 2013). The complex architecture (e.g., Kraus and Middleton, 1987) and wide variety of fluvial environments, from single and multistory channels, to levees, crevasse

splays, and distal floodplain paleosols, as well as facies modified by halokinesis of underlying Paleozoic salt (Woody, 2006; Olsen et al., 2018), means that facies changed rapidly laterally, making lithostratigraphic correlation challenging, even over short distances with excellent outcrop (e.g., Martz and Parker, 2010: fig. 4).

In the vicinity of PFNP, five members of the Chinle Formation are exposed (from oldest to youngest): the Shinarump Conglomerate and Mesa Redondo Member, Blue Mesa Member, Sonsela Member, Petrified Forest Member, and Owl Rock Member (Parker, 2006; Woody, 2006; Martz and Parker, 2010). Following the description by Martz et al. (2012), all five of these lithostratigraphic members are dominated by meandering stream and floodplain deposits but vary in terms of average grain size and sandstone/mudrock ratios, color, and fluvial architecture. Whereas the Mesa Redondo Member has approximately equal parts sandstone and mudrock, is predominantly red in color, often contains multi-color mottling, and predominantly inceptisol paleosols, the overlying Blue Mesa Member is dominated by bluish-gray and purple mudrock showing vertisol development and a small number of multi-story sandstone units with complex internal geometry. The Sonsela Member is perhaps the most multicolored member and has an increase in the proportion of sand, with soil horizons dominated by gleyed vertisols; the lower part is predominantly greenish gray and purple with multi-story sandstones, whereas the upper part of the member is more reddish-brown with more single story sands and the appearance of some aridosol soil horizons. The overlying Petrified Forest Member is dominated by red mudrocks developed into aridosols and vertisols with abundant pedogenic carbonate nodules and a few laterally persistent sandstones with abundant internal cross-stratification and ripple lamination. The youngest unit at PFNP, the Owl Rock Member, is most noticeable for its lighter pastel colors, laterally persistent pedogenic carbonate horizons that often form calcretes, and soil horizons that are almost exclusively aridisols (Fig. 2; Dubiel and Hasiotis, 2011; Martz et al., 2012; Nordt et al., 2015; Olsen et al. 2018).

CPCP core 1A (Fig. 1) was recovered from Chinde Point in the northern part of PFNP, just north of the park headquarters (35.085933° N, 109.795500° W. datum NAD83: Olsen et al., 2018). This core has a total length of 520 m core depth (mcd); because it was drilled at a 30° angle from vertical, and because the strata are close to horizontal, the core comprises a thickness of ~450 m stratigraphic depth (msd) (Fig. 2) (Olsen et al., 2018). CPCP core 1A contains all of the above-named members of the Chinle Formation
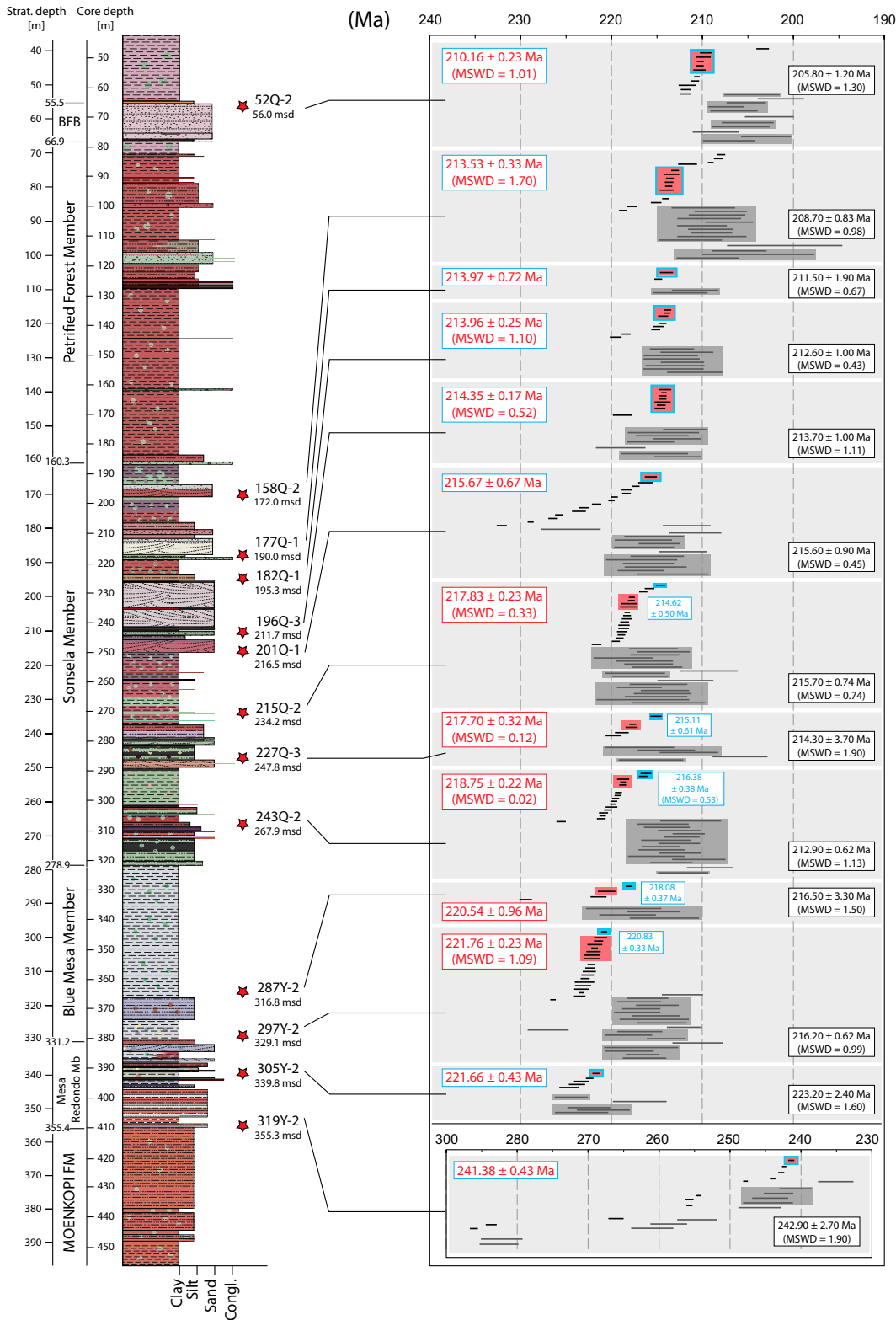
Figure 2. Summary of the U-Pb chemical abrasion–thermal ionization mass spectrometry (CA–TIMS) and laser ablation–inductively coupled plasma–mass spectrometry (LA–ICP–MS) single zircon ages and calculated maximum depositional ages throughout the Colorado Plateau Coring Project (CPCP) core, ranging from the Black Forest Bed of the Chinle Formation to the Moenkopi Formation. Note, from top to bottom, that the CA–TIMS and LA–ICP–MS ages are always obtained from the same zircon crystal, and their position within the age distribution plot reflects this (meaning the top CA–TIMS age corresponds to the top LA–ICP–MS age and so forth). Red boxes with blue rims indicate CA–TIMS ages used for both age models 1 and 2, whereas red boxes represent ages used in age model 1 and blue boxes indicate ages used in age model 2. Gray boxes indicate LA–ICP–MS ages included within the calculation of weighted mean ages. Red stars indicate sampling location within the stratigraphic section. MSWD—mean square of weighted deviates; msd—meters stratigraphic depth.

except the Shinarump Conglomerate (which is a basal lateral facies of the Mesa Redondo Member), and the upper part of the Owl Rock Member, but it also includes the entire underlying, unconformably bound, Lower–Middle Triassic Moenkopi Formation and the top of the Upper Permian Coconino Sandstone, as well as the unconformably overlying Miocene Bidahochi Formation. The Chinle Formation is recovered between a stratigraphic core depth of 20.6 m and 355.4 m and has a total stratigraphic thickness of 334.8 m. In the core, the stratigraphic thicknesses of the Chinle members are as follows (from bottom to top): Mesa Redondo Member, 24.2 m; Blue Mesa Member, 52.3 m; Sonsela Member,

118.6 m; Petrified Forest Member, 118.6 m. The Black Forest marker bed occurs 93.4 m above the base of the Petrified Forest Member and at a stratigraphic depth of 66.9–55.5 m, and the Owl Rock Member begins at a stratigraphic depth of 21.1 m (based on Kent et al., 2018). We note that these lithostratigraphic boundaries may or may not be age-equivalent laterally (see also File S1[1]).

Finally, the Chinle Formation is unconformably underlain by the Moenkopi Formation in CPCP core 1A with a stratigraphic core depth between 359.9 m and 447.4 m and a total stratigraphic thickness of 87.5 m (based on Kent et al., 2018 and Olsen et al., 2018). The Holbrook Member (stratigraphic thickness 40.5 m) comprises the uppermost part of the Moenkopi in the core and is dominated by reddish-brown siltstones and sandstones with greenish-gray mottles (Fig. 1) and provides the oldest sample examined in this study.

PREVIOUS U-Pb GEOCHRONOLOGY

After few early limited geochronologic studies of the Chinle Formation (Miller and Kulp, 1958, 1963; Peirce et al., 1985), a large volume of U-Pb zircon data were produced from outcrop samples over about the past 20 years, mostly by using laser ablation–inductively coupled plasma–mass spectrometry (LA–ICP–MS) (Riggs et al., 1996; Dickinson and Gehrels, 2008a, 2008b, 2009; Riggs et al., 2012, 2013, 2016; Marsh et al., 2019), but also sensitive high-resolution ion microprobe (SHRIMP) (Riggs et al., 2003), and isotope dilution–thermal ionization mass spectrometry (ID–TIMS) (Riggs et al., 2003; Heckert et al., 2009; Irmis et al., 2011; Ramezani et al., 2011, 2014; Atchley et al., 2013; Nordt et al., 2015; Kent et al., 2018) methods.

The Black Forest Bed in the Petrified Forest Member at PFNP (Ash, 1992) is the most studied interval, with several U-Pb ID–TIMS published ages from this volcaniclastic sandstone. Riggs et al. (2003) reported a weighted mean ID–TIMS cluster age of 213 ± 1.7 Ma based on 12 individual zircon analyses. The single zircon ages are associated with relatively high uncertainties, possibly masking multiple age populations, although the crystals were also not pre-treated with the thermal annealing–chemical abrasion (CA) technique to minimize the effects of Pb loss; Mundil et al., 2004; Mattin-

son, 2005). Heckert et al. (2009) also report a single zircon ID–TIMS age of 211 ± 0.7 Ma for this unit but also did not use CA pre-treatment. The more recent weighted mean cluster age of 209.93 ± 0.26 Ma published by Ramezani et al. (2011) is plausibly more accurate because a relatively large number of crystals were analyzed (N = 16) using the chemical abrasion–isotope dilution–thermal ionization mass spectrometry (CA–TIMS) technique. Other SHRIMP and LA–ICP–MS ages for the Black Forest Bed (e.g., Riggs et al., 2003) are also less reliable because these techniques do not use CA pre-treatment and have higher analytical uncertainties.

Ramezani et al. (2011), Atchley et al. (2013), and Nordt et al. (2015) provide outcrop-based U-Pb CA–TIMS cluster ages for multiple levels throughout the Mesa Redondo, Blue Mesa, Sonsela, and Petrified Forest members of the Chinle Formation from PFNP and surrounding areas. Ramezani et al. (2011) and Atchley et al. (2013) produced maximum depositional ages from the lower Mesa Redondo Member of 225.18 ± 0.28 Ma (SS-28; N = 6) and 227.6 ± 0.08 Ma (SS-24; N = 5), respectively. From the lower Blue Mesa Member, Ramezani et al. (2011) reported a maximum depositional age of 223.04 ± 0.27 Ma (TPs; N = 7), and Atchley et al. (2013) published a weighted mean cluster age for the upper part of the member of 220.12 ± 0.07 Ma (SS-7; N = 6). Ramezani et al. (2011) reports five U-Pb CA–TIMS ages for the Sonsela Member ranging from 219.32 ± 0.27 Ma (SBJ; stratigraphically lowest; N = 6) to 213.12 ± 0.27 Ma (GPU; stratigraphically highest; N = 5), and Nordt et al. (2015) published a CA–TIMS zircon cluster age of 213.63 ± 0.28 Ma (P57C; N = 3) from the upper Sonsela Member (Mountain Lion Mesa outcrop) at PFNP. The only age constraints these authors published for the Petrified Forest Member in PFNP are the aforementioned Black Forest Bed age of 209.93 ± 0.26 Ma (BFB, N = 5) and a poorly resolved age from a horizon above this unit of ≤207.8 Ma (SS-37, N = 1).

Most recently, our research group (Kent et al., 2018) published four high precision U-Pb CA–TIMS ages for the upper third of the CPCP drill core 1A from the upper part of the Sonsela Member and Petrified Forest Member as part of a study testing the stability of the 400 k.y. eccentricity cycle. These ages include a weighted mean age for the Black Forest Bed of 210.08 ± 0.22 Ma (52Q-2; N = 6) and three upper Sonsela Member ages (bottom to top): 214.08 ± 0.20 Ma (182Q-1; N = 6); 212.81 ± 1.25 Ma (177Q-1; N = 1); and 213.55 ± 0.28 Ma (158Q-2; N = 9). (See Results section of this paper for further discussion of these data.)

In summary, based on published CA–TIMS geochronologic age constraints from outcrops, the Chinle Formation at PFNP was deposited between 227.6 Ma and 207.8 Ma (or later), is Norian in age, and almost certainly extends into the Rhaetian based on the considerable thickness of strata overlying the youngest dated horizon. That said, in the PFNP area, these important age constraints do not fully resolve chronostratigraphic issues because the stratigraphic superposition of the ages were determined by lateral correlation of short outcrop sequences, whose relationship among each other is not always clear (e.g., Martz and Parker, 2010). Thus, ages from the CPCP core are necessary to build an age model with reduced uncertainties.

A few U-Pb CA–TIMS ages are also available for the Chinle Formation outside of the PFNP area. Irmis et al. (2011) report a weighted mean cluster age of 218.7 ± 0.2 Ma (N = 9) for the lower Chinle Formation at Six Mile Canyon in western New Mexico and a maximum deposition age of 211.9 ± 0.7 Ma for the Petrified Forest Member from the Hayden Quarry at Ghost Ranch in northern New Mexico. Ramezani et al. (2014) report several U-Pb CA–TIMS cluster ages from the lower Chinle Formation of eastern Arizona and western New Mexico. These included an age of 219.39 ± 0.28 Ma (N = 5) from the *Placerias* Quarry in the lower Chinle Formation south of St. Johns, Arizona, an age of 218.42 ± 0.26 Ma (N = 4) from a sandstone bed located ~14 m higher in the same section, and a maximum depositional age of ≤221.6 Ma from the Blue Mesa Member near Salado, Arizona. They also provided a cluster age of 220.73 ± 0.28 Ma (N = 3) from near the base of the Bluewater Creek Member and two younger single zircon ages of 219.9 Ma and 219.3 Ma from 35 m to 45 m higher in the unit at Bluewater Creek, New Mexico (see also Parker, 2018, and Marsh et al., 2019, for stratigraphic interpretation of those sections).

A large number of U-Pb LA–ICP–MS detrital zircon ages from sandstones have been published by Dickinson and Gehrels (2008a, 2008b, 2009), Riggs et al. (2012, 2013, 2016), and more recently by Gehrels et al. (2020) from CPCP core 1A of the Chinle Formation. U-Pb ages ranged from Late Archean to Late Triassic. Due to the relatively large analytical uncertainty associated with the LA–ICP–MS analyses (≥2%), lack of pre-treatment to minimize Pb loss, and thus the likely effects of averaging several different age populations yielding inaccurate ages, they are not well suited for detailed depositional age constraints or stratigraphic correlations (Russ and Baven, 1987; Jarvis

et al., 1991; Rehkämper et al., 2001). However, these data are extremely valuable for provenance studies by determining the age inventory of hundreds to thousands of crystals per sample and identifying which horizons and individual crystals should be targeted for more precise CA–TIMS analyses.

MATERIAL AND METHODS

Thirteen volcaniclastic-bearing siltstone and sandstone samples (data on four of the samples were previously published by Kent et al., 2018) from every ~20 m throughout the Chinle Formation part of CPCP core 1A were analyzed in this study (see also Gehrels et al., 2020). The zircon mineral separation was conducted at the Arizona LaserChron Center using standard techniques adjusted for the relatively small (quarter core width, 20 cm in length), often clay rich, core samples (see also Gehrels, 2000; Gehrels et al., 2008; Gehrels and Pecha, 2014). The samples were separated by hand crushing, hand panning for initial density separation, and with an ultrasonic disruptor (Hoke et al., 2014) to separate the zircon minerals from clays. This was followed by magnetic separation with a Frantz Isodynamic separator and heavy liquids separation with the aid of methylene iodide.

The individual zircons were mounted on 2.5 cm epoxy mounts under the microscope by hand or by pouring to obtain a statistically relevant age inventory of each sample. The unknowns were analyzed against the primary zircon standard FC-1, and two secondary standards (SL and R33). The zircon mounts were exposed using hand polishing (depth: 5–10 μm) to image the internal crystal structures with the aid of a backscatter electron (BSE) detector system using a Hitachi S3400 scanning electron microscope (SEM). A shallow polishing depth was chosen in order to preserve as much zircon material as possible for the subsequent CA–TIMS analysis while also allowing us to avoid inclusions or fractures for the LA–ICP–MS analysis. Prior to the LA–ICP–MS analysis the mounts were cleaned with 1% hydrochloric acid (HCl) and 1% nitric acid (HNO$_3$).

The LA–ICP–MS zircon U-Pb isotope analyses were conducted using a Teledyne Photon Machines Analyte G2 laser connected to a Thermo Element 2 mass spectrometer. Analyses utilized a 20 μm diameter spot with a laser frequency of 7 Hz for 15 seconds, resulting in 10–12 μm deep ablation pits.

The data reduction and subsequent age calculation was conducted with the aid of an in-house data reduction routine (E2agecalc) following the methods of Pullen et al. (2018). The results were filtered for discordance (using cut-offs of 80% and 105% concordance), precision (10%), and common Pb (>600 cps counts of ^{204}Pb). All analytical data are reported in Table S1 (see footnote 1). For each sample, ~80–300 zircon crystals were analyzed. (Further details of the analytical set-up are reported by Gehrels et al., 2020).

Due to the relatively higher uncertainty associated with the LA–ICP–MS analyses (≥2%) the youngest age population (usually 10–15 zircon crystals) was chosen for the more precise (~0.1%) U-Pb ID-TIMS method. To minimize the effects of Pb loss (leading to too young ages that are not representative of the true time of crystallization), the individual zircon crystals were pre-treated using the chemical abrasion (CA) technique (Mattinson, 2005) to dissolve parts of the zircon crystals that are most susceptible to open system behavior. The individual zircon crystals were annealed in an oven at 850 °C for 48 h before they were loaded individually into Teflon capsules and leached in hydrogen fluoride (HF) in a pressure vessel in an oven at 220 °C for 12 h. The chemically abraded zircon crystals were cleaned in aqua regia in an ultrasonic bath before repeatedly being rinsed in nitric acid. Finally the individual zircon crystals were placed again in Teflon capsules and were spiked with a ^{205}Pb-^{233}U-^{235}U tracer solution (either in house Berkeley Geochronology Center (BGC) tracer or Earthtime ET535 tracer; for intercalibration see Irmis et al., 2011, and Griffis et al., 2018) before the sample was finally dissolved in HF in a pressure vessel in an oven at 220 °C for 72 h. After dissolution the individual samples were mixed with phosphoric acid and loaded with silica gel on a filament prior to degassing. The U-Pb CA–TIMS analyses were conducted on a Micromass Sector 54 TIMS at the Uranium Daughter Laboratory at the BGC. Uranium isotopes were measured as oxide. Isotopic ratios were measured using peak hopping.

The data reduction, correction, and error calculation were conducted using Tripoli and U-Pb_Redux (Bowring et al., 2008; McLean et al., 2008) as well as Isoplot (Ludwig, 2012). The ^{206}Pb/^{238}U dates are used for age interpretation because they are more precise than the ^{207}Pb/^{235}U dates due to the low abundance of ^{207}Pb (Schoene et al., 2006; Mattinson, 2010; Ramezani et al., 2011). All analytical data are reported in Table S2 (see footnote 1).

Maximum depositional ages were obtained based on the youngest coherent U-Pb age cluster in a sample (consisting of at least three single crystal ages + n) from which a weighted mean age was calculated. If no coherent age cluster could be observed, the youngest one or two crystal ages within a sample were interpreted as a preliminary maximum depositional age (Fig. 2). Ages that display signs of residual Pb loss (such as unusually young, non-reproducible ages) were excluded because they may be inaccurate.

Finally, with aid of the statistical software R, we employed the StalAge algorithm (Version 1.0) (Scholz and Hoffmann, 2011) to calculate an age model based on the maximum depositional ages defined by the youngest coherent age cluster, their uncertainty, and stratigraphic depth. (Note, preliminary ages based on single crystal U-Pb ages were excluded from this calculation). The StalAge algorithm identifies major/minor outliers (and factors in an increased uncertainty for minor outliers) and age inversions within the data set before calculating an age model (out of subsets of the data set) with a Monte Carlo simulation (95% confidence) including an uncertainty envelope (here in gray [Fig. 3] or yellow [Fig. 4]) (Scholz and Hoffmann, 2011).

RESULTS

Maximum depositional ages for samples 52Q-2, 158Q-2, 177Q-1, and 182Q-1 were recently reported based on weighted mean cluster ages by Kent et al. (2018). The single crystal ages of these four samples are here intercalibrated with the EARTHTIME ET535 tracer. These ages are included in the results section as well. The recalibration has essentially no effect on the correlation or conclusions presented in Kent et al. (2018) or Olsen et al. (2019).

The maximum depositional ages in the results section are based, if possible, on the youngest coherent U-Pb age cluster from which a weighted mean age was calculated. Those ages were employed to construct age model 1 and, in parts, to construct age model 2 (following the magnetostratigraphy-based age model for the CPCP core published by Kent et al., 2019). Further, the maximum depositional ages must follow stratigraphic superposition throughout the section.

The U-Pb LA–ICP–MS and CA–TIMS ages discussed in this study are summarized in Figure 2 and listed in Table 1 (with their core depth in meters [mcd] and their stratigraphic depth in meters [msd]).

Petrified Forest Member

52Q-2

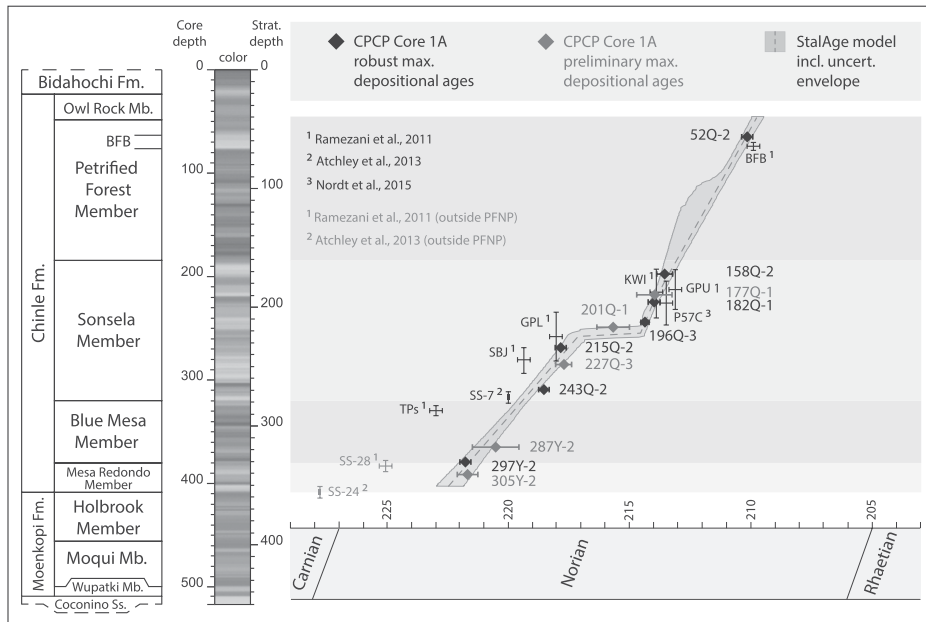This sample is from a 1.7-m-thick (mcd), well sorted, subangular to subrounded, purplish-pink

Figure 3. Correlation of the chemical abrasion–thermal ionization mass spectrometry (CA–TIMS) maximum depositional ages and corresponding age model of the Chinle Formation from Colorado Plateau Coring Project (CPCP) core 1A with the maximum depositional ages published by Ramezani et al. (2011), Atchley et al. (2013), and Nordt et al. (2015) with their estimated stratigraphic uncertainties. Whereas in the upper part of the Chinle core and outcrop ages correspond well with one another, in the lower Chinle Formation the outcrop-based maximum depositional ages from Ramezani et al. (2011), Atchley et al. (2013), and Nordt et al. (2015) have large stratigraphic uncertainties as detailed in File S1 (see footnote 1). Fm.—formation; Mb.—member; Ss.—sandstone; PFNP—Petrified Forest National Park; BFB—Black Forest Bed.

siltstone and fine sandstone that represents the Black Forest Bed of the Petrified Forest Member (64.6 mcd; 56.0 msd).

A total of 302 zircon crystals were analyzed by LA–ICP–MS, and 11 crystals of the youngest age populations were chosen for the CA–TIMS analyses. The LA–ICP–MS ages of these 11 zircon crystals range from 208.5 ± 2.6 Ma to 201.4 ± 2.5 Ma from which a weighted mean age of 205.8 ± 1.2 Ma (mean square of weighted deviates [MSWD] = 1.3; N = 8) was calculated. The two youngest crystals (201.4 ± 2.5 Ma; 202.6 ± 2.7 Ma) and the oldest one (208.5 ± 2.6 Ma) are excluded from the calculation because their uncertainties did not overlap with the main age cluster and may reflect different zircon populations.

The CA–TIMS ages range from 211.85 ± 0.60 Ma to 203.38 ± 0.69 Ma. A weighted mean cluster age of 210.16 ± 0.23 (MSWD = 1.01; N = 5) was calculated and interpreted as the maximum depositional age (for both age models 1 and 2). The youngest crystal, with an age of 203.38 ± 0.69, is excluded because it is unreproducible and could stem from residual Pb loss.

The Th/U ratios in parts per million (ppm) of this sample range from 0.38 to 1.97, suggesting the zircon crystals derived from different magmatic sources.

Sonsela Member

158Q-2

This sample is from a 3.6-m-thick (mcd), moderately sorted, subangular to subrounded, dark reddish-brown to light gray, fine to medium sandstone from the upper Sonsela Member (~10 mcd below the top) (198.6 mcd; 172.0 msd).

A total of 224 zircon crystals were analyzed by LA–ICP–MS, and the 14 crystals of the youngest age population were chosen for the CA–TIMS analyses. The LA–ICP–MS ages of these 14 crystals range from 211.3 ± 3.5 Ma to 201.0 ± 6.3 Ma, from which a weighted mean age of 208.7 ± 0.83 (MSWD = 0.98; N = 13) was calculated. The youngest crystal (201.0 ± 6.3 Ma) is excluded from this calculation because its uncertainty does not overlap with the main age cluster.

The CA–TIMS ages range from 218.74 ± 0.45 Ma to 207.97 ± 0.46 Ma. A weighted mean cluster age of 213.53 ± 0.33 (MSWD = 1.7; N = 6) was calculated and interpreted as the maximum depositional age (and used for both age models 1 and 2). Four younger single zircon ages (211.63 ± 1.04 Ma; 209.09 ± 0.32 Ma; 208.32 ± 0.52; 207.97 ± 0.46) were excluded as they either did not form a coherent age cluster or because their ages are younger than the maximum depositional age calculated for the overlying Black Forest Bed and therefore contradict stratigraphic order within the maximum depositional ages proposed here, as well as those of previous findings. Because those four ages also do not form an age plateau (overlapping with one another in uncertainty), they could reflect residual Pb loss.

The Th/U ratios (ppm) of this sample range from 0.70 to 1.66, suggesting the zircon crystals were derived from different magmatic sources.

177Q-1

This sample is from a 0.6-m-thick (mcd), moderately sorted, subrounded to rounded green siltstone to sandy siltstone of the upper Sonsela Member (219.4 mcd; 190.0 msd).

A total of 237 zircon crystals were analyzed by LA–ICP–MS, and two crystals of the youngest age population were chosen for the CA–TIMS analyses. The LA–ICP–MS ages of these two zircon crystals range from 212.4 ± 3.0 Ma to 210.8 ± 2.6 Ma, from which a weighted mean age of 211.5 ± 1.9 Ma (MSWD = 0.67; N = 2) was calculated.

The CA–TIMS ages are 214.87 ± 0.43 Ma and 213.97 ± 0.72 Ma. The crystals do not form a coherent plateau age, also due to the small sample size, and therefore the youngest zircon crystal with an age of 213.97 ± 0.72 Ma (N = 1) is interpreted as a preliminary maximum depositional age (used in age models 1 and 2). (Note the previous preliminary single crystal age of 212.81 ± 1.25 Ma [Kent et al., 2018] was excluded due to its high analytical uncertainty).

The Th/U ratios (ppm) of this sample range from 0.64 to 1.85, suggesting the crystals stem from different magmatic sources.

182Q-1

This sample is from a 10-m-thick (mcd), grayish red-brown fine sandstone to sandy siltstone of the upper Sonsela Member (225.5 mcd; 195.3 msd).

A total of 279 zircon crystals were analyzed by LA–ICP–MS, and eight crystals of the youngest age population were chosen for CA–TIMS analysis. The LA–ICP–MS ages of these eight zircon crystals range from 219.1 ± 2.7 Ma to 211.9 ± 2.7 Ma, from which a weighted mean
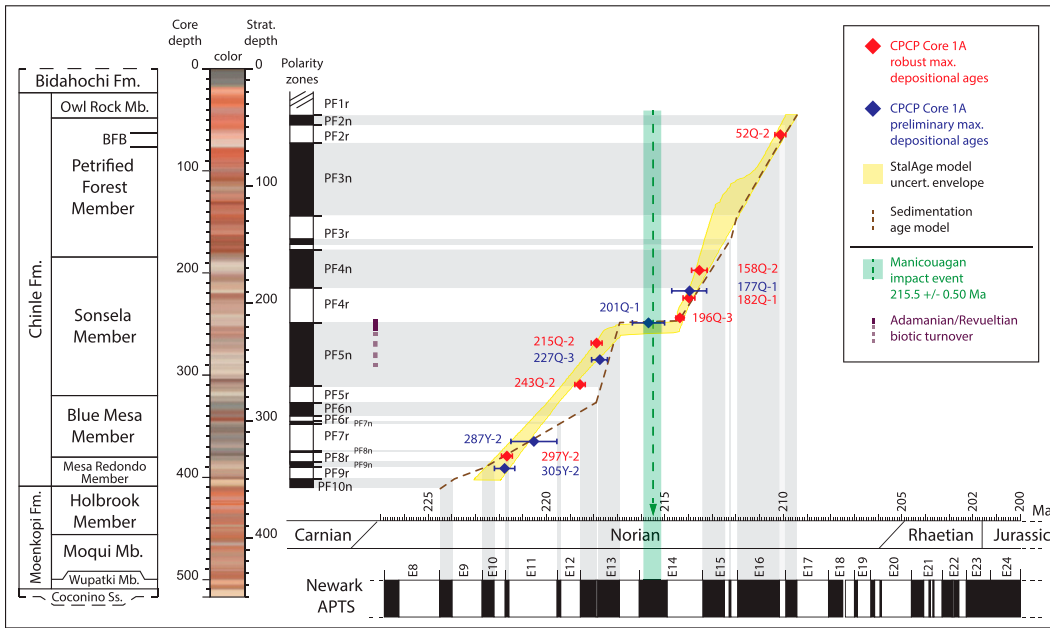
Figure 4. Model 1: Correlation of the chemical abrasion–thermal ionization mass spectrometry (CA–TIMS) maximum depositional ages and corresponding age model of the Chinle Formation from the Colorado Plateau Coring Project (CPCP) core 1A with the magnetostratigraphy of the CPCP core (Kent et al., 2018; Kent et al., 2019) as well as the Newark astronomically calibrated time scale (Kent et al., 2017). The age model assumes that the maximum depositional ages of the Chinle Formation obtained from CPCP core 1A are close to the true depositional age of the strata. This model indicates that the mid-Sonsela Member preserves a condensed section or even an unconformity. Fm.—formation; Mb.—member; Ss.—sandstone; BFB—Black Forest Bed.

age of 212.6 ± 1.0 Ma (MSWD = 0.43; N = 8) was calculated.

The CA–TIMS ages range from 219.54 ± 0.65 Ma to 213.84 ± 0.41 Ma. A weighted mean cluster age of 213.96 ± 0.25 Ma (MSWD = 1.10; N = 3) was calculated from the youngest coherent age plateau and interpreted as the maximum depositional age (for age models 1 and 2).

The Th/U ratios (ppm) of this sample range from 0.49 to 1.05, indicating that the zircon populations originated from different magmatic sources.
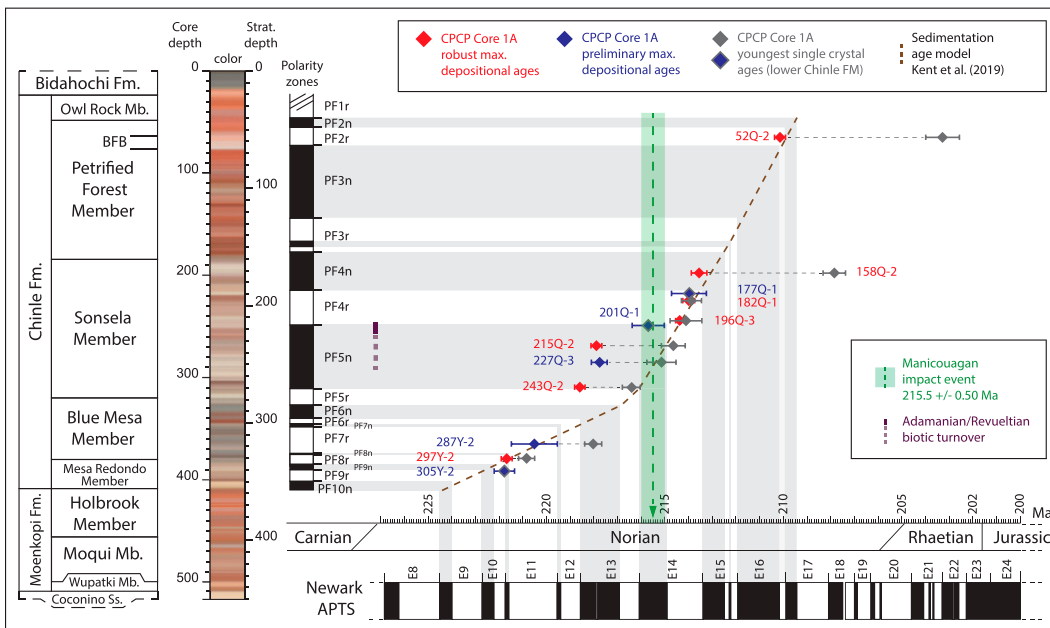

Figure 5. Model 2: Correlation of the CA–TIMS maximum depositional ages and corresponding age model of the Chinle Formation from the CPCP core with the magnetostratigraphy of the CPCP core (Kent et al., 2018; Kent et al., 2019) as well as the Newark astronomically calibrated time scale (Kent et al., 2017). The age model assumes that the maximum depositional ages of the lower Chinle Formation are not representative of the true depositional age of the strata, and therefore, suggests no unconformity in the mid-Sonsela Member but rather a continuous average sediment accumulation rate throughout the Chinle Formation, allowing for an uninterrupted correlation of the magnetostratigraphy of the CPCP core 1A and the Newark–Hartford Astrochronostratigraphic Polarity Time Scale (N–H APTS). Gray (and grayish-blue) diamonds represent the youngest single crystal ages (two youngest crystals for sample 248Q-2) for CPCP core 1A obtained in the Chinle Formation. Blue diamonds with gray rims represent preliminary maximum depositional ages also employed in age model 1. Note that these ages are not reproducible and could stem from residual Pb loss. However, if they reflect younger age populations, they may indicate that the true depositional ages for the lower Chinle Formation might be younger and may correspond with model 2. Fm.—formation; Mb.—member; Ss.—sandstone; BFB—Black Forest Bed.

TABLE 1. SUMMARY OF MAXIMUM DEPOSITIONAL AGES

Sample ID	Member	Core depth (m)	Stratigraphic depth (m)	$^{206}Pb/^{238}U$ age (Ma) Error (2σ)*	MSWD	N
52Q-2	Top Black Forest Bed	64.6	56.0	210.16 ± 0.23	1.01	5
158Q-2	Sonsela Member (10 m below top)	198.6	172.0	213.53 ± 0.33	1.70	6
177Q-1	Sonsela Member	219.4	190.0	213.97 ± 0.72	x	1
182Q-1	Sonsela Member	225.5	195.3	213.96 ± 0.25	1.10	3
196Q-3	Sonsela Member	244.5	211.7	214.35 ± 0.17	0.52	7
201Q-1	Sonsela Member	150.0	216.5	215.67 ± 0.67	x	1
215Q-2	Sonsela Member	270.4	234.2	217.83 ± 0.23 (214.62 ±0.50)*	0.33 (x)*	4 (1)*
227Q-3	Sonsela Member	286.1	247.8	217.70 ± 0.32 (215.11 ±0.61)*	0.12 (x)*	2 (1)*
243Q-2	Sonsela Member (10 m above base)	309.3	267.9	218.57 ± 0.22 (216.38 ±0.38)*	0.023 (0.53)*	3 (2)*
287Y-2	Blue Mesa Member	365.8	316.8	220.54 ± 0.96 (218.08 ±0.37)*	x (x)*	1 (1)*
297Y-2	Blue Mesa Member	380.0	329.1	221.76 ± 0.23 (220.83 ±0.33)*	1.09 (x)*	7 (1)*
305Y-2	Mesa Redondo Member	392.3	339.8	221.66 ± 0.43	x	1
319Y-2	Moenkopi Formation	410.3	355.3	241.31 ± 0.44	x	1

Note: MSWD—mean square of weighted deviates. N—number of crystals.
*Age constraints for age model 2.

196Q-3

This sample is from a 1.2-m-thick (mcd), moderately sorted, planar bedded, subangular to subrounded light grayish-green silty fine sandstone of the lower Sonsela Member (244.5 mcd; 211.7 msd).

A total of 281 zircon crystals were analyzed by LA–ICP–MS, and eight crystals of the youngest age population were chosen for the CA–TIMS analyses. The LA–ICP–MS ages of these eight zircon crystals range from 219.1 ± 2.7–211.9 ± 2.4, from which a weighted mean age of 213.7 ± 1.0 Ma (MSWD = 1.11; N = 7) was calculated. The oldest crystal (219.1 ± 2.7 Ma) is excluded from this calculation because its uncertainty does not overlap with the main age cluster.

The CA–TIMS ages range from 218.80 ± 1.05 Ma to 214.09 ± 0.65 Ma. A weighted mean cluster age of 214.35 ± 0.17 Ma (MSWD = 0.52; N = 7) from a coherent age cluster was calculated and interpreted as the maximum depositional age (for both age models 1 and 2). One older, single crystal age (218.80 ± 1.05 Ma) was excluded because its uncertainty did not overlap with the main age cluster.

The Th/U ratios (ppm) of this sample range from 0.62 to 1.32, indicating that the zircon populations come from different magmatic sources.

201Q-1

This sample is from a 3.87-m-thick (mcd), poorly sorted, angular to subangular reddish-gray to light greenish-gray medium to coarse sandstone of the lower Sonsela Member (250.0 mcd; 216.5 msd).

A total of 262 zircon crystals were analyzed by LA–ICP–MS, and 14 crystals of the youngest age population were chosen for CA–TIMS analysis. The LA–ICP–MS ages of these 14 zircon crystals range from 224.5 ± 3.3 Ma to 210.8 ± 2.8 Ma, from which a weighted mean age of 215.6 ± 0.9 Ma (MSWD = 0.45; N = 10) has been calculated. The three youngest crystals (210.8 ± 2.8 Ma; 211.7 ± 2.6 Ma; 212.2 ± 2.6 Ma) and the oldest one (224.5 ± 3.3 Ma) are excluded from this calculation because their uncertainties do not overlap with the main age cluster, and they might stem from different zircon age populations.

The CA–TIMS ages range from 232.07 ± 0.56 Ma to 215.67 ± 0.67 Ma. The CA–TIMS data display a relatively extensive age spread and do not form a coherent age cluster. Therefore, the youngest crystal age of 215.67 ± 0.67 Ma (N = 1) is interpreted as a preliminary maximum depositional age in age model 1, but is inconsistent with age model 2.

The Th/U ratios (ppm) of this sample range from 0.31 to 1.45, indicating that the zircon populations come from different magmatic sources.

215Q-2

This sample is from a 0.25-m-thick (mcd), moderately sorted, subangular, light greenish-gray medium to coarse sandstone of the lower Sonsela Member (270.4 mcd; 234.2 msd).

A total of 315 zircon crystals was analyzed by LA–ICP–MS, and 18 crystals of the youngest age population were chosen for the CA–TIMS analyses. The LA–ICP–MS ages of these 18 crystals range from 218.7 ± 3.3 Ma to 209.3 ± 3.2 Ma, from which a weighted mean age of 215.7 ± 0.74 Ma (MSWD = 0.74; N = 16) was calculated. The two youngest crystals (209.3 ± 3.2 Ma; 211.9 ± 3.1 Ma) are excluded from this calculation because their uncertainties do not overlap with the main age cluster.

The CA–TIMS ages range from 221.65 ± 0.53 Ma to 214.62 ± 0.50 Ma. A weighted mean cluster age of 217.83 ± 0.23 Ma (MSWD = 0.33; N = 4) has been calculated and interpreted as the maximum depositional age for age model 1. Three younger ages (216.52 ± 0.46 Ma; 215.82 ± 0.53 Ma; 214.62 ± 0.50 Ma) might stem from residual Pb loss because they do not follow stratigraphic order (if one accepts the preliminary age of *201Q-1*), and they do not form a coherent age plateau. However, the youngest grain is consistent with age model 2.

The Th/U ratios (ppm) of this sample range from 0.69 to 1.21, indicating that the zircon populations come from different magmatic sources.

227Q-3

This sample is from the 0.5-m-thick (mcd), well sorted, subangular to subrounded light reddish-gray to light greenish-gray fine to medium sandstone of the lower part of the Sonsela Member (286.1 mcd; 247.8 msd).

A total of 300 zircon crystals were analyzed by LA–ICP–MS, and five zircons of the youngest age population were chosen for the CA–TIMS analyses. The LA–ICP–MS ages of the five zircon crystals range from 216.9 ± 3.8 Ma to 205.9 ± 3.0 Ma, from which a weighted mean age of 214.3 ± 3.7 Ma (MSWD = 1.90; N = 4) was calculated. The youngest crystal (205.9 ± 3.0 Ma) is excluded from this calculation because its uncertainty does not overlap with the main age cluster.

The CA–TIMS ages range from 219.81 ± 0.84 Ma to 215.11 ± 0.61 Ma. The CA–TIMS ages do not form a coherent age cluster, and a preliminary weighted mean age of 217.70 ± 0.32 Ma (MSWD = 0.12; N = 2) can be calculated from two single crystal ages, which is consistent with age model 1. One younger single crystal age (215.11 ± 0.61) was excluded as a preliminary maximum depositional age since it contradicts stratigraphic order with sample 215Q-2, from which we

obtained a robust cluster age, and if one accepts the preliminary age of 201Q-1. However, this youngest crystal age would be consistent with age model 2.

The Th/U ratios (ppm) of this sample range from 0.56 to 1.41, indicating that the zircon populations come from different magmatic sources.

243Q-2

This sample is from a 1.2-m-thick (mcd), purplish-gray sandy silt- to fine sandstone from the lower Sonsela Member (~10 m above base) (309.3 mcd; 267.9 msd).

A total of 305 zircon crystals were analyzed by LA–ICP–MS, and 16 zircons of the youngest age population were chosen for the CA–TIMS analyses. The LA–ICP–MS ages of these 16 zircon crystals range from 215.1 ± 3.1 Ma to 209.2 ± 2.5 Ma, from which a weighted mean age of 212.9 ± 0.62 Ma (MSWD = 1.13; N = 15) was calculated. The youngest crystal (209.2 ± 2.5 Ma) is excluded from this calculation because its uncertainty does not overlap with the main age cluster.

The CA–TIMS ages range from 225.55 ± 0.51 Ma to 216.22 ± 0.59 Ma. A weighted mean cluster age of 218.75 ± 0.22 Ma (MSWD = 0.023; N = 3) was calculated and interpreted as the maximum depositional age. Two younger ages (216.50 ± 0.51 Ma; 216.22 ± 0.59 Ma) could be attributed to residual Pb loss because they do not form a robust age plateau and they also contradict stratigraphic order (within the maximum depositional- and preliminary ages for age model 1 proposed here). However, these two crystal ages are consistent with age model 2.

The Th/U ratios (ppm) of this sample range from 0.58 to 1.59, suggesting the zircon crystals stem from different magmatic sources.

Blue Mesa Member

287Y-2

This sample is from a 7.6-m-thick (mcd), well sorted, subangular to subrounded, bluish-gray with occasional light greenish-gray zones and mottles, finely horizontally laminated siltstone (365.8 mcd; 316.8 msd).

A total of 78 zircon crystals were analyzed by LA–ICP–MS, and four zircon crystals of the youngest age population were chosen for the CA–TIMS analyses. The LA–ICP–MS ages of these four zircon crystals range from 218.7 ± 4.1 Ma to 214.2 ± 3.8 Ma, from which a weighted mean age of 216.5 ± 3.3 Ma (MSWD = 1.50, N = 4) was calculated.

The CA–TIMS ages range from 229.44 ± 0.70 Ma to 218.08 ± 0.33 Ma. The

CA–TIMS ages do not form a coherent age cluster, and therefore the second youngest single crystal age of 220.54 ± 0.96 Ma was interpreted as a preliminary maximum depositional age for age model 1. For age model 1, the one younger crystal age (218.08 ± 0.37 Ma) was excluded because it contradicts stratigraphic order with robust calculated cluster ages and preliminary ages higher in section, and it might stem from residual Pb loss. However, this youngest crystal age is consistent with age model 2.

The Th/U ratios (ppm) of this sample range from 0.58 to 2.16, indicating that the zircon crystals stem from different magmatic sources while the latter is potentially an outlier.

297Y-2

This sample is from a 1.8-m-thick (mcd), well sorted, subangular to subrounded, planar bedded dark reddish-brown siltstone with occasional wispy horizontal light gray streaks (380.0 mcd; 329.1 msd).

A total of 314 zircon crystals were analyzed by LA–ICP–MS, and 19 zircon crystals of the youngest age population were chosen for the CA–TIMS analyses. The LA–ICP–MS ages of these 19 zircon crystals range from 227.0 ± 2.3 Ma to 210.6 ± 2.8 Ma, from which a weighted mean age of 216.2 ± 0.62 Ma (MSWD = 0.99; N = 15) was calculated. The three youngest crystals (210.6 ± 2.8 Ma; 212.0 ± 1.9 Ma; 212.2 ± 2.3 Ma) and the oldest one (227.0 ± 2.3 Ma) are excluded from this calculation because their uncertainties do not overlap with the main age cluster and might stem from different age populations.

The CA–TIMS ages range from 226.43 ± 0.31 Ma to 220.83 ± 0.33 Ma. A weighted mean cluster age of 221.76 ± 0.23 Ma (MSWD = 1.09, N = 7) has been calculated from the youngest age plateau and was interpreted as maximum depositional age and is consistent with both age models 1 and 2. The youngest crystal age of 220.83 ± 0.33 Ma was excluded because it does not overlap in uncertainty with the main age cluster and may suffer from residual Pb loss, although its uncertainty allows it to be close to consistent with age model 2.

The Th/U ratios (ppm) of this sample range from 0.48 to 1.64, suggesting the zircon crystals stem from different magmatic sources.

Mesa Redondo Member

305Y-2

This sample is from a 0.2-m-thick (mcd), poorly sorted, angular to subrounded multi-colored moderate gray, moderate to dark

reddish-brown, purple, greenish-gray, and yellow siltstone to fine sandstone (392.3 mcd; 339.8 msd).

A total of 314 zircon crystals were analyzed by LA–ICP–MS, and five zircons of the youngest age population were chosen for the CA–TIMS analyses. The LA–ICP–MS ages of these five zircon crystals range from 224.4 ± 1.8 Ma to 216.9 ± 3.0 Ma, from which a weighted mean age of 223.2 ± 2.4 Ma (MSWD = 1.6, N = 4) was calculated. The youngest crystal (216.9 ± 3.0 Ma) is excluded from this calculation because its uncertainty does not overlap with the main age cluster.

The CA–TIMS ages range from 229.67 ± 1.44 Ma to 221.66 ± 0.43 Ma. Because none of the CA–TIMS ages form a coherent age cluster but rather a "tail" of ages, the age of the youngest crystal, 221.66 ± 0.43 Ma, is interpreted as a preliminary maximum depositional age consistent with age models 1 and 2. This age was not included in our age model calculation for age model 1 but is marginally consistent with age model 2.

The Th/U ratios (ppm) of this sample range from 0.44 to 1.23, suggesting that the zircon crystals of this sample stem from different magmatic sources.

Moenkopi Formation

319Y-2

This sample is from a 2-m-thick (mcd), very well sorted, subangular to rounded, slightly bedded reddish-brownish-gray silt- to fine sandstone of the Holbrook Member, 0.5 m below the contact with the base of the Chinle Formation (410.3 mcd; 355.3 mbs).

A total of 298 zircon crystals were analyzed by LA–ICP–MS, and 11 crystals of the youngest age population were chosen for CA–TIMS analyses. The LA–ICP–MS ages of these 11 zircon crystals range from 282.6 ± 2.7 Ma to 235.1 ± 2.5 Ma, from which a weighted mean age of 242.9 ± 2.7 Ma (MSWD = 1.90, N = 4) was calculated, based on the youngest coherent age cluster.

The CA–TIMS ages range from 286.10 ± 0.56 Ma to 241.38 ± 0.43 Ma. Because the ages do not form a coherent age cluster, the youngest single crystal age of 241.38 ± 0.43 Ma is interpreted as the maximum depositional age. This age was not included in our age model calculation because it is a single age separated by a widely recognized unconformity from the overlying samples.

The Th/U ratios (ppm) of this sample range from 0.42 to 1.33, indicating that the zircon populations come from different magmatic sources.

DISCUSSION

Comparison of LA–ICP–MS versus CA–TIMS Data

In the absence of obvious primary volcaniclastic deposits (i.e., ashfalls, pyroclastic flows, etc.), it has become increasingly common to utilize the U-Pb ages of redeposited/detrital zircon crystals as a means of extracting maximum depositional ages from non-marine sedimentary strata (e.g., Dickinson and Gehrels, 2009; Irmis et al., 2011; Ramezani et al., 2011; Trujillo et al., 2014; Kohút et al., 2018; D'Emic et al., 2019). Because such samples can comprise a diverse and complex set of age inventories extending into the Proterozoic, LA–ICP–MS is an attractive method given its cost effectiveness and analytical efficiency in evaluating a large number of zircon crystals. In contrast, CA–TIMS offers much higher precision and the ability to minimize the problem of Pb loss, but this approach is at a significant disadvantage in cost and lab throughput. Therefore, an outstanding question has been how maximum depositional ages compare in redeposited samples analyzed using LA–ICP–MS versus CA–TIMS methods. Our study affords the opportunity to directly compare depositional age constraints calculated from both LA–ICP–MS and CA–TIMS analyses of the same material using a large data set (13 samples comprising a total of 135 individual crystals) in which the same zircon crystals were analyzed using both methods. For both LA–ICP–MS and CA–TIMS, we directly compared the single zircon ages and used coherent zircon age clusters to calculate maximum depositional ages by generating one final age from a zircon population. This final cluster age is often associated with a lower uncertainty than is given by the individual analyses, which is especially important for LA–ICP–MS ages that by nature are associated with a higher uncertainty ($\geq$2%) (Russ and Baven, 1987; Rehkämper et al., 2001; Gehrels et al., 2008).

Comparison of the LA–ICP–MS and CA–TIMS single zircon ages (Fig. 2) demonstrates that ages associated with a relatively high uncertainty (independent of whether they were obtained by LA–ICP–MS or CA–TIMS) tend to mask separate age populations that can bias calculated mean ages, given that these calculations assume the crystals come from a single age population. This behavior is particularly apparent in samples 52Q-2, 158Q-2, 215Q-2, 243Q-2, and 297Y-2, where the CA–TIMS ages form a cluster significantly older than the LA–ICP–MS ages (Fig. 2). Therefore, the effect of Pb loss on apparent ages within individual samples can be highly variable. It appears that most zircon crystals from the Chinle Formation experienced some form of Pb loss causing apparent U-Pb ages that are on average too young (e.g., Mattinson, 2005). This is even the case for some CA–TIMS analyses, which becomes apparent within a few samples where single crystal ages had to be excluded from the maximum depositional ages, because they contradicted stratigraphic order (within the array of maximum depositional ages calculated in this study) or deviated too strongly from apparent trends (e.g., samples 52Q-1, 158Q-2, 215Q-2, 243Q-2, and 297Y-2). As a result, a total of 15.4% of the CA–TIMS single crystal ages had to be excluded from those five samples. This relatively high fraction yielding younger and inaccurate individual ages may be due to selecting the zircon fraction based on the youngest LA–ICP–MS ages and thus enhanced radiation damage and Pb loss, even though crystals with unusually high U concentrations were omitted. The U concentration within zircon crystals, which were subsequently picked for the CA–TIMS analyses, ranges from 23 to 915 ppm with most of the crystals having a U concentration of 50–300 ppm (note: the U concentration was obtained during the LA–ICP–MS analysis and therefore reflects the trace element concentration at the ablation spot) (Table S1 [see footnote 1]). Although the LA–ICP–MS ages show a link between increased U concentration and younger ages, the CA–TIMS ages do not reflect the same pattern (Tables S1–S2 [see footnote 1]). This is not surprising, because, due to CA treatment, radiation damaged zones were, at least partly, removed from the crystals. However, it may be possible that residual Pb loss could have been reduced if not only the very youngest zircon tail had been chosen for the CA–TIMS analysis, but rather also older crystals from the entire Late Triassic age distribution. This hypothesis requires further testing. Some samples did not form coherent age clusters at all, which may also be due to residual Pb loss within some of those crystals. This effect also can be observed in previous studies focusing on Chinle strata where U-Pb analyses did not use CA pre-treatment and obtained discordant and comparably younger U-Pb ages (Riggs et al., 2003; Heckert et al., 2009).

Direct comparison of maximum depositional ages, calculated from both the LA–ICP–MS and CA–TIMS data, show that the U-Pb ages retrieved with the LA–ICP–MS method are systematically younger than the U-Pb CA–TIMS ages later obtained from the same zircon crystals, but the offset is variable. In some cases, individual crystal ages show no overlap in uncertainty between the LA–ICP–MS and CA–TIMS values, reinforcing the fact that these analytical uncertainties do not reflect the full geologic uncertainty of the age. The CA–TIMS maximum depositional cluster ages are also typically older than the maximum depositional cluster ages obtained by the LA–ICP–MS analyses, but there is no apparent systematic offset (Fig. 2), which is in agreement with previous studies that applied LA–ICP–MS and CA–TIMS analyses to the same crystals (e.g., Herriott et al., 2019). The difference between the CA–TIMS and LA–ICP–MS ages can be quite small (e.g., 182Q-1 and in particular 196Q-3) or relatively large, such as in samples 52Q-2, 158Q-2, 243Q-2, and 297Y-2, where the maximum depositional ages obtained by LA–ICP–MS are ca. 4.4–5.9 Ma younger, respectively, than those from CA–TIMS. In many cases, however, the combined uncertainty of the LA–ICP–MS samples does overlap with the interpreted depositional age determined using CA–TIMS; for example, in sample 158Q-2 the LA–ICP–MS analyses suggest an age range of ca. 215–201 Ma, which encompasses the cluster age of ca. 213.53 $\pm$ 0.33 Ma interpreted from the CA–TIMS analyses.

Our data suggest that obtaining a reliable maximum depositional age from LA–ICP–MS analyses is not straightforward and that this approach can lead to greater uncertainties than is often appreciated. That said, LA–ICP–MS ages are a powerful tool for efficiently surveying the age inventory of a detrital/redeposited sample, allowing the identification of young crystals for subsequent CA–TIMS analysis. Nonetheless, there is never a guarantee that any analysis, including U-Pb CA–TIMS, has successfully captured the absolute youngest ages, or that the youngest accepted ages are not biased by residual Pb loss, in the stratum of interest.

Age Models for the Chinle Formation

U-Pb and Paleomagnetic Age Models for the CPCP Core

We have developed two conceptually different age models. Model 1 (Fig. 4) assumes that the youngest coherent cluster of zircon U-Pb ages, and the weighted mean ages based on those clusters, best reflects the maximum depositional age of the units. This method has been applied consistently for all samples (see also Kent et al., 2018). Although model 2 employs several of the maximum depositional ages that are based on the youngest coherent age clusters, it also relies on younger, single grain ages, most notably in the lower Sonsela Member, which are presumed to be a trickle of juvenile zircons from syndepositional or at least penecontemporaneous ash falls as cryptotephras residing in the mudstones. However, we do not have objective mechanisms of separating the crystals that may be subject to

unresolved lead loss from those that are truly juvenile.

By introducing additional independent data, such as magnetic polarity, we can test the age models (see also Kent et al., 2019, where the magnetostratigraphy of the CPCP core 1A was introduced). For example, the Petrified Forest–Owl Rock boundary can be constrained to ca. 209.5 Ma because the uppermost Petrified Forest Member comprises a short chron (PF2n), which best correlates with E17n in the N–H APTS (Kent et al., 2018). Similarly, the Sonsela–Petrified Forest boundary is not well-constrained by our U-Pb ages, however, the Sonsela–Petrified Forest boundary is constrained by chron PF4n, which correlates to E15n (N–H APTS) and hence must have an age of 213.4–212.5 Ma (Kent et al., 2018).

Kent et al. (2018) demonstrated that the maximum depositional ages and the paleomagnetic data from the Owl Rock, Petrified Forest, and upper Sonsela members in the core (to a depth of 195 msd), and the ages obtained from outcrop, are consistent with the N–H APTS (Kent et al., 2017), and therefore demonstrated the stability of the 405 k.y. eccentricity cycles extend to ca. 215 Ma. Sample 52Q-2 from the Black Forest Bed has a maximum depositional age of 210.16 ± 0.23 Ma and is within magnetozone PF2r, confirming its correlation to chron E16r in the APTS. Within the upper Sonsela Member, sample 158Q-2 (213.53 ± 0.33 Ma) is within PF4n, correlating to E15n (N–H APTS), and sample 182Q-1 (213.96 ± 0.25 Ma) is within PF4r and correlates to E14r (N–H APTS). The maximum depositional age of 196Q-3 (214.35 ± 0.17 Ma) is also within PF4r and agrees with its correlation to E14r.

However, the zircon U-Pb dates reported here for the lower part of the Sonsela Member in age model 1 are not fully in agreement with the interpretations of the magnetostratigraphy (Kent et al., 2019; here model 2).

Model 1: Assuming that our U-Pb ages based on coherent age clusters from the lower Sonsela Member are close to the depositional age, 215Q-2 (217.83 ± 0.23 Ma) and 243Q-2 (218.75 ± 0.22 Ma) would suggest that PF5n correlates to E13n of the N–H APTS (Fig. 4). This would imply that PF4r correlates to E14r but that E14n and E13r are either unrecorded in core 1A or not sampled. This correlation is consistent with the age of 196Q-3 (214.35 ± 0.17 Ma) from the lower part of PF4r, whose age is consistent with the earliest part of E14r. The preliminary age constraint of 201Q-1 (215.67 ± 0.67 Ma) from the PF4r/PF5n boundary implies that E14n is missing and that PF5n is actually part of E13n. Our single maximum depositional age from the

Blue Mesa Member of 221.76 ± 0.23 Ma (297Y-2) is from chron PF8r, which suggests correlation to E10r (N–H APTS). These maximum depositional ages can be used as anchor points to correlate the remaining CPCP paleomagnetic polarity zones to the N–H APTS (Fig. 4). The inferred age model from these correlations suggests that some of our U-Pb ages from the lower Sonsela Member (i.e., 215Q-2 and 243Q-2) are up to 800 ka older than the depositional age of their constituent strata.

Nonetheless, this correlation is based on the assumption that most of the maximum depositional ages, as we have defined them, obtained from the CPCP core (52Q-2, 158Q-2, 182Q-1, 196Q-3, 215Q-2, 243Q-2, and 297Y-2) are close to the true depositional age of the sedimentary beds (as shown for the upper part of the Chinle Formation [Kent et al., 2018]). If this is correct, the age model implies that one or more hiatus(es) are present within the mid-Sonsela Member, concatenating E13n and E14r as the PF5n/PF4r boundary with no record of E13r and E14n in PFNP. Such an interpretation is consistent with the preliminary age of 201Q-1 (215.67 ± 0.67 Ma), which is significantly older than 196Q-3 (214.35 ± 0.17 Ma) despite being less than 10 msd lower in section. A major implication of age model 1 is that it suggests a very low average sediment accumulation rate (4.5 m/Ma) or even an unconformity for the ~10 m portion of the Sonsela Member from ~218–210 msd. A similar trend was reported by Ramezani et al. (2011), who also inferred a significant drop in average sediment accumulation rate from 24 m/Ma to 28 m/Ma within the Blue Mesa and Petrified Forest Member down to ~5 m/Ma within the mid-Sonsela Member (see also Martz and Parker, 2010).

An obvious question then is whether there is any sedimentologic evidence for such a condensed section in the mid-Sonsela Member. The Sonsela Member as a whole (in core and outcrop) is characterized by mudstones that are frequently and complexly interbedded with (conglomeratic) sandstones and conglomerates with sharp or erosional contacts, down-cutting relationships into underlying strata, reworked sediments at the base, and the increase of pedogenic carbonates within the mid- to upper Sonsela Member (Fig. 2) (Woody, 2006; Parker and Martz, 2010; Martz et al., 2012). These observations also apply for the mid-Sonsela Member in outcrop from which the seemingly abrupt Adamanian–Revueltian biotic turnover has been described, which could be interpreted as a possible hiatus (Woody, 2006; Parker and Martz, 2010; Martz et al., 2012). In CPCP core 1A the mid-Sonsela Member comprises the strata between ~250–225 m stratigraphic depth

and preserves several 5–10-m-thick sandstone beds (Fig. 2) with erosional bases. Unfortunately, we do not know exactly where the Adamanian–Revueltian biotic turnover correlates to in core 1A, and determining this relationship is the subject of ongoing work.

Model 2: This age model is consistent with the magnetostratigraphy of Kent et al. (2019) for the lower half of the CPCP 1A core (Fig. 5), which was completed before the zircon U-Pb ages of the core were available. This CPCP core magnetostratigraphy matches chron-for-chron with the N–H APTS (ending with PF10n being linked to E9n [N–H APTS]). This is consistent with the age and stratigraphic placement of 196Q-3 (214.35 ± 0.17 Ma), which is from the lower part of PF4r, and whose age is consistent with the earliest part of E14r (N–H APTS). This age model implies that no detectable hiatuses or condensed sections (given the analytical approach) are present within the mid-Sonsela Member, but rather that the Chinle Formation preserves two sedimentary regimes with a lower average sediment accumulation rate in the Mesa Redondo and Blue Mesa members (10 m/Ma) and an increased average sediment accumulation rate throughout the Sonsela and Petrified Forest members (34 m/Ma). The stratigraphically bracketing dates in common with model 1 are 214.35 ± 0.17 Ma for sample 196Q-3 from the mid-Sonsela and 221.76 ± 0.23 Ma for sample 297Y-2 from near the base of the Blue Mesa Member; interpretations of the dates in between are dependent on the interpretation of the different age models.

The model 2 correlation implies that the maximum depositional ages from the lower Chinle Formation, as we derive them above, independent if obtained from core or outcrop, tend to be anomalously old and therefore are not close to the true depositional age, but rather reflect older, recycled zircon material (see also Gehrels et al., 2020). For example, if chron PF5n, which extends almost down to the base of the Sonsela Member, is correlated to E14n (N–H APTS) the base of the member should not be older than ca. 216 Ma. However, all U-Pb ages from the lower part of the Sonsela Member in the core (and outcrop; Fig. 3) are older than this date estimate. This suggests that samples 215Q-2, 227Q-3, and 243Q-2 are all 2–2.5 Ma older than their depositional ages. This discrepancy could be explained by a non-preservation or non-detection in the samples of the youngest age population reflecting the true time of deposition. It has to be noted that because the upper Chinle Formation can be well correlated to the N–H APTS with both U-Pb ages and paleomagnetics in agreement (Kent et al., 2018, 2019), it could be considered peculiar that the lower Chinle Formation does

not, with either a missing chron (model 1) or U-Pb ages that don't reflect depositional ages (model 2).

Currently, model 2 cannot be refuted nor validated with certainty by U-Pb maximum depositional ages that are based on coherent cluster ages (independent if based on core or outcrop). However, if taking the entire age spread of the individual samples of the lower Chinle Formation from CPCP core 1A into consideration (Fig. 2), the youngest crystal age of sample 215Q-2 (214.62 ± 0.50 Ma), 227Q-3 (215.11 ± 0.61 Ma), 243Q-2 (2 zircons: 216.38 ± 0.38 Ma [MSWD: 0.53]), and 287Y-2 (218.08 ± 0.37 Ma) would be consistent with model 2 (Fig. 5). Hence, if those single crystal ages were to correspond to a younger age population, either not well captured by our analyses or rare within the zircon population of the sampled sandstone beds, the lower Chinle Formation would correlate as effortlessly with the N–H APTS as the upper Chinle Formation (Figs. 4 and 5) (Kent et al., 2018). However, these ages are only based on single crystal dates (although there are two in the case of sample 243Q-2) that are not reproducible and might indicate residual Pb loss. Therefore, the currently available U-Pb data do not provide unequivocal evidence that younger zircon age populations are preserved within those strata; however, the single crystal ages may be considered as an indicator that younger populations could be present that would reflect the "true" time of deposition. To evaluate if this is the case, additional sampling and zircon analyses are indispensable for clarifying if younger zircon age populations are preserved. We suggest that mudstones within CPCP core 1A could be sampled as an additional source to detect ash fall zircon crystals in cryptotephras that may not be immediately apparent in such rocks because bioturbation might disrupt original bedding of the ashes and mix them with the surrounding mud and silt sediments. In addition, outcrop sampling and additional drilling initiatives would provide further age constraints and hopefully aid in further development of age models for the Chinle Formation.

Depositional Age Constraints based on the Two Age Models

Our U-Pb ages span a time interval of ca. 11.5 Ma for the Chinle Formation in the CPCP core. Age model 1 predicts an overall duration of ca. 15.4 Ma for the Chinle Formation in core 1A, from the basal Owl Rock Member (20.8 msd) to the unconformable base of the Mesa Redondo Member (359.0 msd). This duration also applies to age model 2, because the oldest and youngest ages are the same in both models, spanning an age of ca. 224.25 Ma to ca. 208.9 Ma, suggesting that the entire Chinle Formation in the core is Norian in age based on the current Late Triassic timescale (e.g., Kent et al., 2017). Presumably the Norian–Rhaetian boundary is above the level sampled by core 1A well within the Owl Rock Member based on the inferred numerical age of 205.7 Ma for this boundary (cf. Wotzlaw et al., 2014; Maron et al., 2015; Kent et al., 2017). The age of the base of the Chinle Formation in the core is constrained by a single crystal age of 221.66 ± 0.43 Ma (305Y-2) from the middle of the Mesa Redondo Member, and our age models 1 and 2 predict an age of ca. 224.25 Ma for the preserved base of the formation. This is somewhat younger than the ages of ca. 225 Ma and ca. 227 Ma from the Mesa Redondo Member published by previous authors from sites southeast of PFNP in Hunt Valley 25 km southeast of PFNP (Ramezani et al., 2011; Atchley et al., 2013). Because it is not possible to unambiguously correlate between either the CPCP core 1A or outcrops at PFNP, it is entirely possible that these ages are accurate, even if we cannot assess them using our core data.

The Mesa Redondo–Blue Mesa Member boundary is constrained by the aforementioned date and the overlying date of 221.76 ± 0.23 Ma (297Y-2 [Fig. 2]). The inferred age of this boundary is ca. 221.90 Ma based on our age models 1 and 2, suggesting an age duration of ca. 2.40 Ma for the Mesa Redondo Member. The top of the Blue Mesa Member is only constrained by a preliminary single crystal age of 220.54 ± 0.96 Ma (287Y-2) and a maximum depositional age of 218.75 ± 0.22 Ma (243Q-2) from the lower Sonsela Member. The age model 1 suggests a date of ca. 217.75 Ma for the Blue Mesa–Sonsela boundary and a duration of ca. 4.2 Ma for the Blue Mesa Member, whereas age model 2 suggests an age of ca. 216.80 Ma for the boundary and an overall duration of ca. 5.1 Ma for this member. Again, given the uncertainty of the stratigraphic correlation between outcrop and core, and the ambiguity of assessing the relative stratigraphic positions of outcrop samples based on different published sections, it is not possible to objectively assess the differences between these outcrop-based ages and our age models (Fig. 3) (see also File S1 [see footnote 1]). It is also worth noting that the previous Mesa Redondo ages (SS-28 [Ramezani et al., 2011], SS-24 [Atchley et al., 2013]) (Fig. 3) come from Hunt Valley, located 25 km southeast of PFNP, so there are significant ambiguities with lithostratigraphic correlation, and it is plausible that the top of the Mesa Redondo Member varies in age across its geographic extent.

Based on our U-Pb data, the Sonsela Member spans at least ca. 5.22 Ma from 218.75 ± 0.22 Ma (243Q-2) to 213.53 ± 0.33 Ma (158Q-2). Here the lower part of the member is defined at/or below a core depth of 244.5 m (stratigraphic depth at/below 211.7 m). Above this depth carbonate nodules become much more abundant, and this feature has also been used to define the upper and lower part of the Chinle Formation (e.g., Martz et al., 2012). The lower Sonsela Member was deposited between ca. 217.75 Ma (age model 1) and ca. 216.80 Ma (age model 2) to 214.35 ± 0.17 Ma (196Q-3) (age models 1 and 2), and therefore had a duration of ca. 3.4 Ma (age model 1) or ca. 2.45 Ma (age model 2). The U-Pb ages for the upper part of the member ranged from 214.35 ± 0.17 Ma (196Q-3) to 213.53 ± 0.33 Ma (158Q-2). For the Sonsela Member–Petrified Forest Member boundary both age models predict an age of ca. 212.70 Ma, lasting for at least ca. 1.65 Ma.

Previously published PFNP outcrop ages for the lower part of the Sonsela Member cannot be placed in objective correlation with the core because different authors place the sample levels in very different positions (e.g., the Jasper Forest Bed, that produced sample GPL, is 25 m lower in Parker and Martz (2010) than in Atchley et al. (2013) relative to the base of the Blue Mesa Member [see File S1; see footnote 1]). In contrast, for the upper Sonsela and Petrified Forest members, outcrop ages fall largely within the uncertainties of our core ages (Fig. 3) (Ramezani et al., 2011; Nordt et al., 2015; Kent et al., 2018), plausibly because they are from outcrops in the northern part of the park, close to the core, while the discrepant ages are nearly entirely from the southern section of the park.

Implications for Depositional History

The proposed age models allow us to calculate average sediment accumulation rates throughout the depositional history of the Chinle Formation in core 1A. Crucially, some of these sedimentation rates depart significantly from the models proposed in previous studies for the same Chinle strata at PFNP (e.g., Ramezani et al., 2011; Howell and Blakey, 2013). Both age models 1 and 2 agree on the age and duration of the Petrified Forest Member, upper Sonsela Member, lower Blue Mesa Member, and Mesa Redondo Member. Where the age models differ is in the upper Blue Mesa–lower Sonsela interval; model 1 suggests the Blue Mesa–Sonsela boundary is ca. 217.75 Ma in age, whereas model 2 suggests this boundary is ca. 216.80 Ma in age. As discussed above, this is because model 1 implies a mid-Sonsela condensed section and rapid accumulation of the lower Sonsela/uppermost Blue Mesa members, but model 2 implies a rapid accumulation of the entire Sonsela Member and a relatively slower accumulation of the Blue Mesa Member.

As a result, age model 1 predicts a fairly consistent average sediment accumulation rate of ~12 m/Ma (360–285 msd) for the Mesa Redondo through upper Blue Mesa members, a much higher average sediment accumulation rate of ~67 m/Ma (285–218 msd) for the uppermost Blue Mesa through lower Sonsela members, and a rate of ~36 m/Ma (210.5–40 msd) for the upper Sonsela Member through lowermost Owl Rock Member. In stark contrast, the middle part of the Sonsela Member possesses a much slower average sedimentation rate of ~4.5 m/Ma (218–210.5 msd). As noted, these data suggest either a strongly condensed section for this interval and/or the presence of one or more unconformities/depositional hiatuses.

Previous age models and model 2 for these strata suggested a slower depositional rate in the lower Chinle Formation of ~10 m/Ma (360–270 msd) and an increased rate in the upper part of the formation of ~34 m/Ma (270–40 msd), with a single inflection point somewhere within the middle Sonsela Member (Ramezani et al. 2011; Howell and Blakey, 2013) or at the base of the Sonsela Member (Kent et al., 2019).

However, model 1 suggests that rather than a relatively continuous section with an increase in sedimentation rate, a key 8 m part of the Sonsela Member is highly condensed and possibly incomplete. Crucially, this interval is closely associated with the observed biotic turnover at PFNP as allowed by the bracketing ages in model 1, the age of the Manicouagan impact event, and regional climatic and tectonic shifts inferred by other authors based on these previous models (e.g., Atchley et al., 2013; Nordt et al., 2015) may not be recorded in PFNP strata. In contrast, if the average sediment accumulation rates predicted by model 2 are correct (10 m/Ma for the Mesa Redondo and Blue Mesa Members and 34 m/Ma for the Sonsela and Petrified Forest Members [34 m/Ma]), the time of the Manicouagan impact event would be preserved in the lower Sonsela Member somewhere between ~240–265 msd (see section below on implications for biotic and climate events).

Age of the Moenkopi Formation

The complex age inventory of our sample from the uppermost Holbrook Member of the Moenkopi Formation makes it difficult to interpret, but these data are nonetheless significant because they are the first CA–TIMS ages from the formation. The youngest crystal age of 241.38 ± 0.48 Ma (N = 1) is not reproduced by any other crystal analysis, so it could represent Pb loss. This age is very close to the most recent Anisian–Ladinian boundary age of 241.464 ± 0.064 (Wotzlaw et al., 2018). Nonetheless, a number of crystals preserve

ages of 242–244 Ma, suggesting this horizon has a maximum depositional age younger than 245 Ma. These data suggest the top of the Moenkopi Formation is middle–late Anisian or even earliest Ladinian in age (Ogg, 2012; Storck et al., 2019) and therefore younger than the traditional early Anisian age inferred for this part of the formation (e.g., Morales, 1987; Hunt et al., 1993; Steiner et al., 1993; Lucas and Schoch, 2002). Still, it is consistent with the interpretation that a significant regional unconformity of ~10–12 m.y. is present at the Moenkopi–Chinle contact in this area (e.g., Stewart et al., 1972a, 1972b, 1978; Pipiringos and O'Sullivan, 1978; Dickinson and Gehrels, 2008a).

Implications for Late Triassic Biotic Change and Climatic Events

Our new age models for the Chinle Formation at PFNP have implications for the interpretation of regional and global events during the Norian Stage of the Late Triassic Epoch.

It has long been established that the Chinle Formation preserves several distinct vertebrate assemblages (e.g., Camp, 1930; Gregory, 1957; Colbert and Gregory, 1957; Long and Ballew, 1985; Lucas, 1991, 1993; Lucas and Hunt, 1993; Lucas et al. 2007). At PFNP, the boundary of two vertebrate biozones, the Adamanian and Revueltian, is preserved within the mid-Sonsela Member (e.g., Parker and Martz, 2010, 2017; Martz and Parker, 2017). This vertebrate turnover appears to be correlated with a palynofloral turnover at PFNP (Litwin et al., 1991; Parker, 2006; Parker and Martz, 2010; Reichgelt et al., 2013; Baranyi et al., 2018), and this biotic turnover is associated with a persistent red "silcrete" layer in the lower Jim Camp Wash beds that authors have used as a lithostratigraphic marker for this biostratigraphic event (e.g., Parker and Martz, 2010).

Ramezani et al. (2011) constrained the Adamanian–Revueltian turnover to mid-upper Norian, between 219 Ma (SBJ) and 213 Ma (GPU). As such, a number of authors have suggested that this turnover could be associated with the Manicouagan impact event in Quebec, Canada (Mundil and Irmis, 2008; Olsen et al., 2010; Parker and Martz, 2010), which is dated to ca. 215.5 Ma (Ramezani et al., 2005). Alternatively, other authors have concluded this biotic change was a result of climate change to more arid conditions, either as a result of Pangaea drifting northward out of the equatorial humid zone (Kent and Tauxe, 2005; Whiteside et al., 2010; Dubiel and Hasiotis, 2011) or the development of the Cordilleran magmatic arc, which caused an enhanced rain shadow effect (Atchley et al., 2013), and some have even suggested it

is an artifact of the incompleteness of the stratigraphic record and/or fossil sampling (Heckert and Lucas, 1996; Hayes et al., 2020).

Outcrop data indicate the biotic turnover is within the middle third of the Sonsela Member (Parker and Martz, 2010; Martz and Parker, 2017). Using this as a conservative constraint, our age model 1 (Fig. 4) suggests the middle third of the Sonsela Member was deposited between ca. 217.5–214 Ma. This overlaps in age with the Manicouagan impact but also suggests that the biotic turnover could be located within a stratigraphic interval that is a condensed section. In this case, it is possible that the turnover was relatively gradual but appears sudden because of one or more unconformities, depositional hiatuses, or very low average accumulation rates. Age model 2 (Fig. 5) suggests this part of the Sonsela Member was deposited between ca. 215.7 and 214 Ma but with a relatively constant average depositional rate. This would imply that the sudden biotic turnover is a real pattern and that it may have coincided with the age of the Manicouagan impact.

Regardless of the preferred age model, inferring a more precise age for the biotic turnover requires a precise (i.e., sub-meter) and accurate stratigraphic correlation between outcrop and core. Paleomagnetic data indicate that the impact event occurred during a time of normal polarity (Robertson, 1967; Larochelle and Currie, 1967; Eitel et al., 2016), plausibly chron E14n in the N–H APTS, whereas the paleomagnetic polarity of the outcrop red silcrete horizon itself is not clear, as it is located between normal and reversed polarity samples (cf. Zeigler et al., 2017: fig. 7). Regardless of the precise age of the turnover, these new age constraints for the Chinle Formation further confirm that the Adamanian and Revueltian vertebrate biozones and Zone II and III palynofloral biozones are Norian in age (see also Irmis et al., 2010, 2011, for discussion) and not late Carnian–early Norian as suggested by Lucas (1998, 2010) and Lucas et al. (2007). Equally important, they demonstrate clearly that the fossil-bearing part of the Chinle Formation in the PFNP area postdates the middle Carnian, and thus cannot preserve any evidence of the Carnian Pluvial Event, an asserted global sudden warming event, in contrast with the suggestions of some recent authors (e.g., Lucas and Tanner, 2018; Baranyi et al., 2019).

Correlation to Other Key Upper Triassic Records

Our new age models for the Chinle Formation at PFNP allow refined correlation to Chinle strata elsewhere on the Colorado Plateau that have precise geochronologic age constraints

(e.g., Irmis et al., 2011; Ramezani et al., 2014). As previously discussed by Kent et al. (2018), an age range of ca. 212.5–211 Ma for the lower half of the Petrified Forest Member is consistent with the CA–TIMS U-Pb detrital zircon age of 211.9 ± 0.7 Ma from the Hayden Quarry (Irmis et al., 2011), which is from the lowermost part of the same lithostratigraphic unit in northern New Mexico. This confirms that the early dinosaur-bearing sites in the lower Petrified Forest Member of both areas, which share similar taxonomic content (Irmis et al., 2007; Parker and Martz, 2010), are of similar age. Regional correlations can also be revised using our new U-Pb ages from the lower Chinle Formation. Irmis et al. (2011) reported a CA–TIMS age of 218.1 ± 0.7 Ma from a unit they considered to be near the base of the Blue Mesa Member in Bluewater Creek, western New Mexico (however, see discussion in Marsh et al., 2019) and correlated it with the base of the Sonsela Member at PFNP. In our age model 1, this date also correlates with the lowermost Sonsela Member at PFNP, and the reversed polarity zone of the upper Bluewater Creek Member (e.g., Irmis et al., 2011: fig. 3) would correlate with PF5r. Age model 2 would place this date in the upper Blue Mesa Member and correlate the reversed zone to PF6r. Finally, Ramezani et al. (2014) reported a number of new CA–TIMS ages between ca. 221.6 Ma and 218.4 Ma from the lower Chinle Formation of easternmost Arizona and western New Mexico, including a classic vertebrate fossil site, the *Placerias* Quarry. The dated strata in these sections had previously been correlated to the Mesa Redondo and lower Blue Mesa members (Heckert and Lucas, 2003a, 2003b), but Ramezani et al. (2014) and Parker (2018) suggested instead that they correlated to the younger uppermost Blue Mesa and Sonsela members at PFNP. Our new age models are consistent with a correlation of the youngest ages of these strata (218.4 ± 0.07 Ma at Romero Springs, Arizona, and ≤219.3 Ma at Bluewater Creek, New Mexico) to either the upper Blue Mesa Member or lowermost Sonsela Member. In contrast, the oldest ages from the lowermost part of these sections (≤221.6 Ma at Salado, Arizona, and 220.73 ± 0.12 Ma at Bluewater Creek, New Mexico) best correlate to the lower part of the Blue Mesa Member at PFNP. Thus, these data support the hypothesis that the early dinosaurs from the *Placerias* Quarry are not significantly older than the oldest dinosaur records from PFNP, which come from the middle Blue Mesa Member (Irmis et al., 2011; Parker and Martz, 2010).

The integration of U-Pb ages and magnetostratigraphy from the CPCP core at PFNP allows for a much more refined correlation of the fossil records from the Colorado Plateau in western North America to those of the Newark Supergroup in eastern North America (e.g., Olsen et al., 2002, 2010, 2015; Sues and Olsen, 2015; Whiteside et al., 2011). Specifically, the Chinle Formation at PFNP correlates with the New Oxford–Lockatong and Lower Passaic–Heidlersburg palynomorph biozones (Kent et al., 2017: fig. 1), which are wholly Norian in age. This confirms previous correlations suggesting that some key palynomorph taxa have diachronous ranges across the two regions (Reichgelt et al., 2013; Lindström et al., 2016; Baranyi et al., 2018). In particular, the last appearances of *Infernopollenites claustratus*, *Cycadopites stonei*, and *Lagenella martini* are all between 220 Ma and 212 Ma (middle–late Norian) in the Chinle Formation, but their last appearances in the Newark are between 227 Ma and 225 Ma in either the top of the Richmond–Taylorsville or lowermost New Oxford–Lockatong biozones (Lindström et al., 2016; Baranyi et al., 2018; Kent et al., 2017). It is worth noting, however, that the New Oxford–Lockatong biozones are very sparsely sampled. Similarly, *Camerosporites secatus* is present as late as 211 Ma (late Norian) in the Chinle Formation, but its last appearance in the Newark is the lower New Oxford–Lockatong biozone, which is no younger than ca. 222 Ma (Lindström et al., 2016; Kent et al., 2017). Again, though, the lower part of the overlying Lower Passaic–Heidlersberg biozone is very sparsely sampled.

The fossiliferous part of the Chinle Formation at PFNP comprises the Blue Mesa Member through the lowermost Owl Rock Member (Parker and Martz, 2010; Martz and Parker, 2017), which based on our age models dates to ca. 221.5–209 Ma (middle–late Norian). This corresponds well to the footprint and vertebrate body fossil record from the Newark Supergroup published by Olsen et al. (2002), which begins in chron E10r, dated to ca. 222 Ma (Kent et al., 2017). Both the Newark and Chinle records confirm that dinosaurs were rare (i.e., low relative abundance), species-poor, and limited to small- to medium-size theropods (i.e., no ornithischians or sauropodomorphs) throughout the Norian–Rhaetian in low-latitude North America, in contrast with mid- and high-latitude Late Triassic assemblages of the same age (Irmis, 2011; Irmis et al., 2011; Olsen et al., 2010; Whiteside et al., 2015; Kent et al., 2014, 2017). The Blomidon Formation in the Fundy Basin, Nova Scotia correlates to E15n through E23n of the N–H APTS (Kent and Olsen, 2000; Whiteside et al., 2011) and thus ranges in age from ca. 213 Ma to 201.6 Ma (Kent et al., 2017). Thus, the uppermost Sonsela Member through lowermost Owl Rock Member of the Chinle Formation at PFNP

correlates with the lower part of the Blomidon Formation. The Blomidon vertebrate assemblage comprises both footprints included in the Olsen et al. (2002) study and a fragmentary body fossil record that includes the procolophonid reptile *Hypsognathus*, isolated archosauriform teeth, and phytosaurs (Whiteside et al., 2011; Sues and Olsen, 2015). This limited body fossil record makes detailed comparisons with the Chinle Formation difficult. If the underlying Wolfville Formation is indeed Carnian (Kent and Olsen, 2000; Whiteside et al., 2011; Sues and Olsen, 2015), its extensive tetrabrate body fossil assemblage (Sues and Olsen, 2015) is significantly older than any specimens from the Chinle Formation. Similarly, the late Carnian–early Norian (ca. 233–227 Ma) vertebrate footprints and body fossils from the Pekin and Cumnock formations of the Deep River Basin in North Carolina (Olsen and Huber, 1998; Whiteside et al., 2011; Olsen et al., 2015; Zanno et al., 2015; Heckert et al., 2017) are several million years older than the oldest part of the vertebrate fossil record of the Chinle Formation. The younger "lithofacies association II" from the same basin, which includes dicynodonts, traversodontid cynodonts, aetosaurs, the loricatan archosaur *Postosuchus alisonae*, and the early crocodylomorph *Dromicosuchus grallator* (Sues et al., 2003; Peyer et al., 2008), is plausibly early–middle Norian in age (Whiteside et al., 2011; Olsen et al., 2015), and thus may correlate with the Adamanian biozone (Blue Mesa–lower Sonsela members) of the Chinle Formation, which also includes dicynodonts, aetosaurs, *Postosuchus*, and early crocodylomorphs, but lacks cynodonts (Irmis, 2005; Parker and Martz, 2010). The Cow Branch Formation of the Dan River Basin in North Carolina also correlates to this interval (Whiteside et al., 2011; Olsen et al., 2015), but shared vertebrate taxa are limited to semi-aquatic taxa such as phytosaurs and tanystropheids (Olsen et al., 2015), because the Cow Branch body fossil record largely comprises lacustrine facies, in contrast with the channel and floodplain facies that dominate the Chinle Formation.

The vertebrate biozones of western North America have often been correlated to fossil assemblages in South America, such as the Agua de Peña Group of northwestern Argentina as well as with the Santa Maria and Caturrita formations in southern Brazil (e.g., Rogers, 1997; Lucas, 1998, 2010; Shipman, 2004; Langer, 2005; Lucas et al., 2007; Ramezani et al., 2011). Previous workers suggested that the Adamanian biozone correlates with the Ischigualastian biozone in Argentina and Brazil (e.g., Hunt and Lucas, 1991a, 1991b; Lucas and Hunt, 1993). Our new ages conclusively demonstrate that the

Chinle Formation postdates these units and correlates instead with the overlying Los Colorados Formation (Irmis et al., 2011; Kent et al., 2014, 2018). Thus, the dinosaur fossils of the Chinle Formation are significantly younger than the oldest dinosaurs from South America, which are late Carnian in age (e.g., Rogers et al., 1993; Martinez et al., 2011; Langer et al., 2018). The stratigraphically oldest dinosaur fossils from the Chinle Formation are found in the bone bed of the *Placerias* Quarry in northeastern Arizona (Hunt et al., 1998; Long and Murry, 1995; Lucas et al., 1992; Nesbitt et al., 2007), which as mentioned above, is dated by a high precision U-Pb CA–TIMS cluster age of 219.39 ± 0.28 Ma ($N = 5$) (Ramezani et al., 2014), placing it in the middle Norian. Comparisons with other key Upper Triassic fossil assemblages across Pangaea, such as those found in the Argana Basin of Morocco, lower Elliot Formation of southern Africa, the middle Keuper of the Germanic Basin in central Europe, and Pranhita–Godavari Basin of India, remain difficult because they lack precise geochronologic age constraints from magnetostratigraphy and/or numerical age estimates (e.g., reviews in Irmis, 2011; Irmis et al., 2011).

CONCLUSIONS

Our U-Pb LA–ICP–MS and CA–TIMS ages obtained from the CPCP core of the Upper Triassic Chinle strata demonstrate that LA–ICP–MS ages (and some CA–TIMS ages) associated with a relatively high uncertainty tend to mask age populations within a sample. Moreover, several LA–ICP–MS ages are younger than the CA–TIMS ages of the same crystals, suggesting that these zircon grains experienced Pb loss to various degrees. This emphasizes the importance of precise and accurate single crystal ages using methods that correct for Pb loss (e.g., CA–TIMS) in developing robust U-Pb maximum depositional age constraints.

The here reported U-Pb CA–TIMS chronostratigraphy based on silt- and sandstone beds of the Upper Triassic Chinle Formation confirms that previously published outcrop and CPCP core-based maximum depositional ages correspond well with one another within the upper part of the formation (Kent et al., 2018). In contrast, within the lower Chinle Formation, outcrop-to-outcrop and outcrop-to-core correlation ambiguities make assessment of the similarities or differences between outcrop and core dates equivocal. Nevertheless, the here reported age constraints show that the Sonsela Member of the Chinle Formation was deposited no earlier than 221.76 ± 0.23 Ma and no later than 210.16 ± 0.23 Ma and therefore is entirely Norian in age.

Our data demonstrate that the vertebrate biozones preserved in the Sonsela Member at PFNP are also Norian in age, with the Adamanian–Revueltian boundary being mid Norian in age. This verifies the hypotheses of previous authors (e.g., Irmis et al., 2011; Ramezani et al., 2011; Atchley et al., 2013).

Further, we propose two alternative age models for the Chinle Formation at PFNP. Model 1 assumes that the maximum depositional ages based on the largest, youngest coherent age clusters obtained from the core are close to the true depositional age of the strata, indicating that the sediment accumulation rate was very low (amounting to an unconformity of several million years) within the middle Sonsela Member and that a long N–H APTS polarity zone is missing in the PFNP record. This also implies that the biotic turnover at the Adamanian–Revueltian transition may have occurred rather gradually (see also Hayes et al., 2020). Model 2 suggests a more straightforward correlation of the magnetostratigraphic data to the N–H APTS, with no major polarity zones missing in the PFNP record. This implies that the youngest, largest coherent age clusters of the upper Blue Mesa Member and lower Sonsela Member may reflect redeposited older crystals and are not representative of the depositional age. Hence, they are unsuited for robustly testing the interpretations of the depositional age. This model implies that the mid-Sonsela Member stratigraphic record is relatively complete, that it does preserve a sudden biotic turnover, and allows the possibility that this event correlates to the time of the Manicouagan impact event.

Finally, our study demonstrates the complexities of interpreting depositional age constraints from populations of redeposited zircon crystals but also the power of integrating these data with those from magnetic polarity stratigraphy information to develop testable and accurate age models for sedimentary strata.

REFERENCES CITED

Allen, V.T., 1930, Triassic bentonite of the Painted Desert: American Journal of Science, v. 112, p. 283–288, https://doi.org/10.2475/ajs.s5-19.112.283.

Ash, S., 1992, The Black Forest Bed, a distinctive unit in the Upper Triassic Chinle Formation, northeastern Arizona: Journal of the Arizona–Nevada Academy of Science, v. 24–25, p. 59–73.

Ash, S., 2005, Synopsis of the Upper Triassic flora of Petrified Forest National Park and vicinity: Mesa Southwest Museum Bulletin, v. 9, p. 53–62.

Ash, S.R., 1980, Upper Triassic floral zones of North America, *in* Dilcher, D.L., and Taylor, T.M., eds., Biostratigraphy of Fossil Plants: Stroudsburg, Dowden, Hutchinson and Ross, Inc., p. 153–170.

Atchley, S.C., Nordt, L.C., Dworkin, S.I., Ramezani, J., Parker, W.G., Ash, S.R., and Bowring, S.A., 2013, A linkage among Pangean tectonism, cyclic alluviation, climate change, and biologic turnover in the Late Triassic: The record from the Chinle Formation, southwestern United States: Journal of Sedimentary Research, v. 83, p. 1147–1161, https://doi.org/10.2110/jsr.2013.89.

Baranyi, V., Reichgelt, T., Olsen, P.E., Parker, W.G., and Kürschner, W.M., 2018, Norian vegetation history and related environmental changes: New data from the Chinle Formation, Petrified Forest National Park (Arizona, SW USA): Geological Society of America Bulletin, v. 130, p. 775–795, https://doi.org/10.1130/B31673.1.

Baranyi, V., Miller, C.S., Ruffell, A., Hounslow, M.W., and Kürschner, W.M., 2019, A continental record of the Carnian Pluvial Episode (CPE) from the Mercia Mudstone Group (UK): Palynology and climatic implications: Journal of the Geological Society, v. 176, p. 149–166, https://doi.org/10.1144/jgs2017-150.

Berner, R.A., 2006, GEOCARBSULF: A combined model for Phanerozoic atmospheric O_2 and CO_2: Geochimica et Cosmochimica Acta, v. 70, p. 5653–5664, https://doi.org/10.1016/j.gca.2005.11.032.

Blackburn, T.J., Olsen, P.E., Bowring, S.A., McLean, N.M., Kent, D.V., Puffer, J., McHone, G., Rasbury, E.T., and Et-Touhami, M., 2013, Zircon U-Pb geochronology links the end-Triassic extinction with the Central Atlantic Magmatic Province: Science, v. 340, p. 941–945, https://doi.org/10.1126/science.1234204.

Blakey, R.C., 2008, Gondwana paleogeography from assembly to breakup; A 500 m.y. odyssey: Geological Society of America Special Paper 441, p. 1–28.

Blakey, R.C., and Gubitosa, R., 1983, Late Triassic paleogeography and depositional history of the Chinle Formation, southern Utah and northern Arizona, *in* Reynolds, M.W., and Dolly, E.D., eds., Mesozoic Paleogeography of West-Central United States: Denver, Colorado, Society of Economic Paleontologists and Mineralogists, Rocky Mountain Section, p. 57–76.

Blakey, R.C., and Gubitosa, R., 1984, Controls of sandstone body geometry and architecture in the Chinle Formation

(Upper Triassic), Colorado Plateau: Sedimentary Geology, v. 38, p. 51–86, https://doi.org/10.1016/0037-0738(84)90074-5.

Bowring, S.A., Bowring, J.F., Condon, D., Heizler, M., Johnson, K.R., McLean, N.M., Parrish, R., Ramezani, J., and Schoene, B., 2008, The EARTHTIME initiative: A review of progress and prospects, in Joint Meeting of The Geological Society of America, Soil Science Society of America, American Society of Agronomy, Crop Science Society of America, Gulf Coast Association of Geological Societies with the Gulf Coast Section of SEPM, v. 40, p. 135.

Cadigan, R.A., 1963, Tuffaceous sandstones in the Triassic Chinle Formation, Colorado Plateau: U.S. Geological Survey Professional Paper 475B, p. B48–B51.

Camp, C.L., 1930, A study of the phytosaurs with description of new material from western North America: Memoirs of the University of California, v. 10, p. 1–160.

Cohen, B.E., Mark, D.F., Lee, M.R., and Simpson, S.L., 2017, A new high-precision $^{40}Ar/^{39}Ar$ age for the Rochechouart impact structure: At least 5 Ma older than the Triassic–Jurassic boundary: Meteoritics & Planetary Science, v. 52, p. 1600–1611, https://doi.org/10.1111/maps.12880.

Colbert, E.H., and Gregory, J.T., 1957, Correlation of continental Triassic sediments by vertebrate fossils: Geological Society of America Bulletin, v. 68, p. 1456–1467.

D'Emic, M.D., Foreman, B.Z., Jud, N.A., Britt, B.B., Schmitz, M., and Crowley, J.L., 2019, Chronostratigraphic revision of the Cloverly Formation (Lower Cretaceous, Western Interior, USA): Bulletin of the Peabody Museum of Natural History, v. 60, p. 3–40, https://doi.org/10.3374/014.060.0101.

Dickinson, W.R., and Gehrels, G.E., 2008a, U-Pb ages of detrital zircons in relation to paleogeography: Triassic paleodrainage networks and sediment dispersal across southwest Laurentia: Journal of Sedimentary Research, v. 78, p. 745–764, https://doi.org/10.2110/jsr.2008.088.

Dickinson, W.R., and Gehrels, G.E., 2008b, Sediment delivery to the Cordilleran foreland basin: Insights from U-Pb ages of detrital zircons in Upper Jurassic and Cretaceous strata of the Colorado Plateau: American Journal of Science, v. 308, p. 1041–1082.

Dickinson, W.R., and Gehrels, G.E., 2009, Use of U–Pb ages of detrital zircons to infer maximum depositional ages of strata: A test against a Colorado Plateau Mesozoic database: Earth and Planetary Science Letters, v. 288, p. 115–125, https://doi.org/10.1016/j.epsl.2009.09.013.

Dietz, R.S., and Holden, J.C., 1970, Reconstruction of Pangaea: Breakup and dispersion of continents, Permian to present: Journal of Geophysical Research, v. 75, p. 4939–4956, https://doi.org/10.1029/JB075i026p04939.

Dubiel, R.F., 1994, Triassic deposystems, paleogeography, and paleoclimate of the Western Interior, in Caputo, M.V., Peterson, J. A., and Franczyk, K. J., eds., Mesozoic Systems of the Rocky Mountain Region, USA: Denver, Society of Economic Paleontologists and Mineralogists Rocky Mountain Section, p. 133–168.

Dubiel, R.F., Parrish, J.T., Parrish, J.M., and Good, S.C., 1991, The Pangaean megamonsoon—Evidence from the Upper Triassic Chinle Formation, Colorado Plateau: Palaios, v. 6, p. 347–370, https://doi.org/10.2307/3514963.

Dubiel, R.F., and Hasiotis, S.T., 2011, Deposystems, paleosols, and climatic variability in a continental system: The Upper Triassic Chinle Formation, Colorado Plateau, USA, in Davidson, S.K., Leleu, S., and North, C.P., From River to Rock Record: The Preservation of Fluvial Sediments and Their Subsequent Interpretation: Society for Sedimentary Geology Special Publication 97, p. 393–421.

Eitel, M., Gilder, S.A., Spray, J., Thompson, L., and Pohl, J., 2016, A paleomagnetic and rock magnetic study of the Manicouagan impact structure: Implications for crater formation and geodynamo effects: Journal of Geophysical Research: Solid Earth, v. 121, p. 436–454, https://doi.org/10.1002/2015JB012577.

Falkowski, P.G., Katz, M.E., Knoll, A.H., Quigg, A., Raven, J.A., Schofield, O., and Taylor, F.J.R., 2004, The evolution of modern eukaryotic phytoplankton: Science, v. 305, p. 354–360, https://doi.org/10.1126/science.1095964.

Foster, G.L., Royer, D.L., and Lunt, D.J., 2017, Future climate forcing potentially without precedent in the last 420 million years: Nature Communications, v. 8, p. 1–8, https://doi.org/10.1038/ncomms14845.

Fraser, N.C., and Sues, H.D., 2010, The beginning of the 'Age of Dinosaurs': a brief overview of terrestrial biotic changes during the Triassic: Earth and Environmental Science Transactions of the Royal Society of Edinburgh, v. 101, p. 189–200, https://doi.org/10.1017/S1755691011020019.

Furin, S., Preto, N., Rigo, M., Roghi, G., Gianolla, P., Crowley, J.L., and Bowring, S.A., 2006, High-precision U-Pb zircon age from the Triassic of Italy: Implications for the Triassic time scale and the Carnian origin of calcareous nannoplankton and dinosaurs: Geology, v. 34, p. 1009–1012, https://doi.org/10.1130/G22967A.1.

Gehrels, G., and Pecha, M., 2014, Detrital zircon U-Pb geochronology and Hf isotope geochemistry of Paleozoic and Triassic passive margin strata of western North America: Geosphere, v. 10, p. 49–65, https://doi.org/10.1130/GES00889.1.

Gehrels, G.E., 2000, Introduction to detrital zircon studies of Paleozoic and Triassic strata in western Nevada and northern California, in Soreghan, M.J. and Gehrels, G.E., eds., Paleozoic and Triassic Paleogeography and Tectonics of Western Nevada and Northern California: Geological Society of America Special Paper 347, p. 1–18, https://doi.org/10.1130/0-8137-2347-7.1.

Gehrels, G.E., Valencia, V., and Ruiz, J., 2008, Enhanced precision, accuracy, efficiency, and spatial resolution of U-Pb ages by laser ablation–multicollector–inductively coupled plasma–mass spectrometry: Geochemistry, Geophysics, Geosystems, v. 9, p. 1–13, https://doi.org/10.1029/2007GC001805.

Gehrels, G.E., Giesler, D., Olsen, P.E., Kent, D.V., Marsh, A., Parker, W.G., Rasmussen, C., Mundil, R., Irmis, R.B., Geissman, J.W., and Lepre, C.J., 2020, LA–ICP–MS U-Pb geochronology of detrital zircon grains from the Coconino, Moenkopi, and Chinle Formations in the Petrified Forest National Park (Arizona): Geochronology, https://doi.org/10.5194/gchron-2019-12.

Good, S.C., 1998, Freshwater bivalve fauna of the Late Triassic (Carnian–Norian) Chinle, Dockum, and Dolores Formations of the southwest United States, in Bivalves: An Eon of Evolution: Calgary, University of Calgary Press, p. 223–249.

Greene, A.R., Scoates, J.S., Weis, D., Katvala, E.C., Israel, S., and Nixon, G.T., 2010, The architecture of oceanic plateaus revealed by the volcanic stratigraphy of the accreted Wrangellia oceanic plateau: Geosphere, v. 6, p. 47–73, https://doi.org/10.1130/GES00212.1.

Gregory, J.T., 1957, Significance of fossil vertebrates for correlation of Late Triassic continental deposits of North America. XX Congreso Geologico Internacional, Sección II: El Mesozoico del Hemisferio Occidental y sus Correlaciónes Mundiales: International Geological Congress, Mexico City, p. 7–25.

Grieve, G.A.F., 2006, Impact Structures in Canada: St. John's, Newfoundland, Geological Association of Canada, 210 p.

Griffis, N.P., Mundil, R., Montañez, I.P., Isbell, J., Fedorchuk, N., Vesely, F., Iannuzzi, R., and Yin, Q.Z., 2018, A new stratigraphic framework built on U-Pb single-zircon TIMS ages and implications for the timing of the penultimate icehouse (Paraná Basin, Brazil): Geological Society of America Bulletin, v. 130, p. 848–858, https://doi.org/10.1130/B31775.1.

Hayes, R.F., Puggioni, G., Parker, W.G., Tiley, C.S., Bednarick, A.L., and Fastovsky, D.E., 2020, Modeling the dynamics of a Late Triassic vertebrate extinction: The Adamanian/Revueltian faunal turnover, Petrified Forest National Park, Arizona, USA: Geology, v. 48, p. 318–322, https://doi.org/10.1130/G47037.1.

Heckert, A.B., and Lucas, S.G., 1996, Stratigraphic description of the Tr-4 unconformity in west-central New Mexico and eastern Arizona: New Mexico Geology, v. 18, p. 61–70.

Heckert, A.B., and Lucas, S.G., 2003a, Triassic stratigraphy in the Zuni Mountains, west-central New Mexico: New Mexico Geological Society Guidebook, v. 54, p. 245–262.

Heckert, A.B., and Lucas, S.G., 2003b, Stratigraphy and paleontology of the lower Chinle Group (Adamanian: latest Carnian) in the vicinity of St. Johns, Arizona, in 54th Field Conference, Geology of the Zuni Plateau: New Mexico Geological Society Guidebook, v. 54, p. 281–288.

Heckert, A.B., Lucas, S.G., Dickinson, W.R., and Mortensen, J.K., 2009, New ID–TIMS U-Pb ages for Chinle Group strata (Upper Triassic) in New Mexico and Arizona, correlation to the Newark Supergroup, and implications for the "long Norian": Geological Society of America Abstracts with Programs, v. 41, p. 123.

Heckert, A.B., Fraser, N.C., and Schneider, V.P., 2017, A new species of *Coahomasuchus* (Archosauria, Aetosauria) from the Upper Triassic Pekin Formation, Deep River Basin, North Carolina: Journal of Paleontology, v. 91, p. 162–178, https://doi.org/10.1017/jpa.2016.130.

Herriott, T.M., Crowley, J.L., Schmitz, M.D., Wartes, M.A., and Gillis, R.J., 2019, Exploring the law of detrital zircon: LA–ICP–MS and CA–TIMS geochronology of Jurassic forearc strata, Cook Inlet, Alaska, USA: Geology, v. 47, p. 1044–1048, https://doi.org/10.1130/G46312.1.

Hoke, G., Schmitz, M., and Bowring, S., 2014, An ultrasonic method for isolating nonclay components from clay-rich material: Geochemistry, Geophysics, Geosystems, v. 15, p. 492–498, https://doi.org/10.1002/2013GC005125.

Hönisch, B., Ridgwell, A., Schmidt, D.N., Thomas, E., Gibbs, S.J., Sluijs, A., Zeebe, R., Kump, L., Martindale, R.C., Greene, S.E., Kiessling, W., Ries, J., Zachos, J.C., Royer, D.L., Barker, S., Marchitto, T.M., Jr., Moyer, R., Pelejero, C., Ziveri, P., Foster, G.L., and Williams, B., 2012, The geological record of ocean acidification: Science, v. 335, p. 1058–1063, https://doi.org/10.1126/science.1208277.

Howell, E.R., and Blakey, R.C., 2013, Sedimentological constraints on the evolution of the Cordilleran arc: New insights from the Sonsela Member, Upper Triassic Chinle Formation, Petrified Forest National Park (Arizona, USA): Geological Society of America Bulletin, v. 125, p. 1349–1368, https://doi.org/10.1130/B30714.1.

Hunt, A.P., and Lucas, S.G., 1991a, The *Paleorhinus* biochron and the correlation of the non-marine Upper Triassic of Pangaea: Palaeontology, v. 34, p. 487–501.

Hunt, A.P., and Lucas, S.G., 1991b, A new rhynchosaur from the Upper Triassic of West Texas, and the biochronology of Late Triassic rhynchosaurs: Palaeontology, v. 34, p. 927–938.

Hunt, A.P., Santucci, V.L., Lockley, M.G., and Olson, T.J., 1993, Moenkopi Formation (Middle Triassic, Anisian), Arizona, USA: New Mexico Museum of Natural History and Science Bulletin, v. 3, p. 213–218.

Hunt, A.P., Lucas, S.G., Heckert, A.B., Sullivan, R.M., and Lockley, M.G., 1998, Late Triassic dinosaurs from the western United States: Geobios, v. 31, p. 511–531, https://doi.org/10.1016/S0016-6995(98)80123-X.

Irmis, R., 2005, The vertebrate fauna of the Upper Triassic Chinle Formation in northern Arizona: Mesa Southwest Museum Bulletin, v. 9, p. 63–88.

Irmis, R.B., 2011, Evaluating hypotheses for the early diversification of dinosaurs: Earth and Environmental Science Transactions of the Royal Society of Edinburgh, v. 101, p. 397–426, https://doi.org/10.1017/S1755691011020068.

Irmis, R.B., and Whiteside, J.H., 2010, Newly integrated approaches to studying Late Triassic terrestrial ecosystems: Palaios, v. 25, p. 689–691, https://doi.org/10.2110/palo.2010.S06.

Irmis, R.B., Nesbitt, S.J., Padian, K., Smith, N.D., Turner, A.H., Woody, D., and Downs, A., 2007, A Late Triassic dinosauromorph assemblage from New Mexico and the rise of dinosaurs: Science, v. 317, no. 5836, p. 358–361, https://doi.org/10.1126/science.1143325.

Irmis, R.B., Martz, J.W., Parker, W.G., and Nesbitt, S.J., 2010, Re-evaluating the correlation between Late Triassic terrestrial vertebrate biostratigraphy and the GSSP-defined marine stages: Albertiana, v. 38, p. 40–52.

Irmis, R.B., Mundil, R., Martz, J.W., and Parker, W.G., 2011, High-resolution U–Pb ages from the Upper Triassic Chinle Formation (New Mexico, USA) support a diachronous rise of dinosaurs: Earth and Planetary Science Letters, v. 309, p. 258–267, https://doi.org/10.1016/j.epsl.2011.07.015.

Jarvis, K.E., Gray, A.L., and Houk, R.S., 1991, Handbook of inductively coupled plasma mass spectrometry: Chapman and Hall, 380 p.

Kent, D.V., and Irving, E., 2010, Influence of inclination error in sedimentary rocks on the Triassic and Jurassic apparent pole wander path for North America and implications for Cordilleran tectonics: Journal of Geophysical Research: Solid Earth, v. 115, no. B10, p. 1–25, https://doi.org/10.1029/2009JB007205.

Kent, D.V., and Olsen, P.E., 2000, Magnetic polarity stratigraphy and paleolatitude of the Triassic–Jurassic Blomidon Formation in the Fundy Basin (Canada): Implications for early Mesozoic tropical climate gradients: Earth and Planetary Science Letters, v. 179, p. 311–324, https://doi.org/10.1016/S0012-821X(00)00117-5.

Kent, D.V., and Tauxe, L., 2005, Corrected Late Triassic latitudes for continents adjacent to the North Atlantic: Science, v. 307, p. 240–244, https://doi.org/10.1126/science.1105826.

Kent, D.V., Malnis, P.S., Colombi, C.E., Alcober, O.A., and Martínez, R.N., 2014, Age constraints on the dispersal of dinosaurs in the Late Triassic from magnetochronology of the Los Colorados Formation (Argentina): Proceedings of the National Academy of Sciences of the United States of America, v. 111, p. 7958–7963, https://doi.org/10.1073/pnas.1402369111.

Kent, D.V., Olsen, P.E., and Muttoni, G., 2017, Astrochronostratigraphic polarity time scale (APTS) for the Late Triassic and Early Jurassic from continental sediments and correlation with standard marine stages: Earth-Science Reviews, v. 166, p. 153–180, https://doi.org/10.1016/j.earscirev.2016.12.014.

Kent, D.V., Olsen, P.E., Rasmussen, C., Lepre, C., Mundil, R., Irmis, R.B., Gehrels, G.E., Giesler, D., Geissman, J.W., and Parker, W.G., 2018, Empirical evidence for stability of the 405-kiloyear Jupiter–Venus eccentricity cycle over hundreds of millions of years: Proceedings of the National Academy of Sciences of the United States of America, v. 115, p. 6153–6158, https://doi.org/10.1073/pnas.1800891115.

Kent, D.V., Olsen, P.E., Lepre, C., Rasmussen, C., Mundil, R., Gehrels, G.E., Giesler, D., Irmis, R.B., Geissman, J.W., and Parker, W.G., 2019, Magnetochronology of the entire Chinle Formation (Norian Age) in a scientific drill core from Petrified Forest National Park (Arizona, USA) and implications for regional and global correlations in the Late Triassic: Geochemistry, Geophysics, Geosystems, v. 20, p. 4654–4664, https://doi.org/10.1029/2019GC008474.

Kohút, M., Hofmann, M., Havrila, M., Linnemann, U., and Havrila, J., 2018, Tracking an upper limit of the "Carnian crisis" and/or Carnian stage in the western Carpathians (Slovakia): International Journal of Earth Sciences, v. 107, p. 321–335, https://doi.org/10.1007/s00531-017-1491-8.

Kraus, M.J., and Middleton, L.T., 1987, Dissected paleotopography and base-level changes in a Triassic fluvial sequence: Geology, v. 15, p. 18–21, https://doi.org/10.1130/0091-7613(1987)15<18:DPABCI>2.0.CO;2.

Langer, M.C., 2005, Studies on continental Late Triassic tetrapod biochronology. II. The Ischigualastian and a Carnian global correlation: Journal of South American Earth Sciences, v. 19, p. 219–239, https://doi.org/10.1016/j.jsames.2005.04.002.

Langer, M.C., Ramezani, J., and Da Rosa, Á.A.S., 2018, U-Pb age constraints on dinosaur rise from south Brazil: Gondwana Research, v. 57, p. 133–140, https://doi.org/10.1016/j.gr.2018.01.005.

Larochelle, A., and Currie, K.L., 1967, Paleomagnetic study of igneous rocks from the Manicouagan structure, Quebec: Journal of Geophysical Research, v. 72, p. 4163–4169, https://doi.org/10.1029/JZ072i016p04163.

Lindström, S., Irmis, R.B., Whiteside, J.H., Smith, N.D., Nesbitt, S.J., and Turner, A.H., 2016, Palynology of the upper Chinle Formation in northern New Mexico, USA: Implications for biostratigraphy and terrestrial ecosystem change during the Late Triassic (Norian–Rhaetian): Review of Palaeobotany and Palynology, v. 225, p. 106–131, https://doi.org/10.1016/j.revpalbo.2015.11.006.

Litwin, R.J., Traverse, A., and Ash, S.R., 1991, Preliminary palynological zonation of the Chinle Formation, southwestern USA, and its correlation to the Newark Supergroup (eastern USA): Review of Palaeobotany and Palynology, v. 68, p. 269–287, https://doi.org/10.1016/0034-6667(91)90028-2.

Long, R.A., and Ballew, K.L., 1985, Aetosaur dermal armor from the Late Triassic of southwestern North America, with special reference to material from the Chinle Formation of Petrified Forest National Park: Museum of Northern Arizona Bulletin, v. 54, p. 45–68.

Long, R.A., and Murry, P.A., 1995, Late Triassic (Carnian and Norian) tetrapods from the southwestern United States: New Mexico Museum of Natural History and Science Bulletin, v. 4, p. 1–254.

Lucas, S.G., 1991, Sequence stratigraphic correlation of nonmarine and marine Late Triassic biochronologies, western United States: Albertiana, v. 9, p. 11–18.

Lucas, S.G., 1993, The Chinle Group: revised stratigraphy and biochronology of Upper Triassic nonmarine strata in the western United States: Museum of Northern Arizona Bulletin, v. 59, p. 27–50.

Lucas, S.G., 1998, Global Triassic tetrapod biostratigraphy and biochronology: Palaeogeography, Palaeoclimatology, Palaeoecology, v. 143, p. 347–384, https://doi.org/10.1016/S0031-0182(98)00117-5.

Lucas, S.G., 2010, The Triassic timescale based on nonmarine tetrapod biostratigraphy and biochronology, *in* Lucas, S.G., ed., The Triassic Timescale: Geological Society, London, Special Publication 334, p. 447–500, https://doi.org/10.1144/SP334.15.

Lucas, S.G., and Hunt, A.P., 1993, Tetrapod biochronology of the Chinle Group: New Mexico Museum of Natural History and Science Bulletin, v. 3, p. 327–329.

Lucas, S.G., and Schoch, R.R., 2002, Triassic temnospondyl biostratigraphy, biochronology and correlation of the German Buntsandstein and North American Moenkopi Formation: Lethaia, v. 35, p. 97–106, https://doi.org/10.1080/002411602320183962.

Lucas, S.G., and Tanner, L.H., 2018, Record of the Carnian wet episode in strata of the Chinle Group, western USA: Journal of the Geological Society, v. 175, p. 1004–1011, https://doi.org/10.1144/jgs2017-134.

Lucas, S.G., Hunt, A.P., and Long, R.A., 1992, The oldest dinosaurs: Naturwissenschaften, v. 79, p. 171–172, https://doi.org/10.1007/BF01134434.

Lucas, S.G., Hunt, A.P., Heckert, A.B., and Spielmann, J.A., 2007, Global Triassic tetrapod biostratigraphy and biochronology: 2007 status: New Mexico Museum of Natural History and Science Bulletin, v. 41, p. 229–240.

Ludwig, K.R., 2012, Isoplot 3.75–4.15: A geochronological toolkit for Microsoft Excel: Berkeley Geochronology Center Special Publication, p. 1–75.

Luo, Z.-X., 2007, Transformation and diversification in mammal evolution: Nature, v. 450, p. 1011–1019, https://doi.org/10.1038/nature06277.

Maron, M., Rigo, M., Bertinelli, A., Katz, M.E., Godfrey, L., Zaffani, M., and Muttoni, G., 2015, Magnetostratigraphy, biostratigraphy, and chemostratigraphy of the Pignola–Abriola section: New constraints for the Norian–Rhaetian boundary: Geological Society of America Bulletin, v. 127, p. 962–974, https://doi.org/10.1130/B31106.1.

Marsh, A.D., Parker, W.G., Stockli, D.F., and Martz, J.W., 2019, Regional correlation of the Sonsela Member (Upper Triassic Chinle Formation) and detrital U-Pb zircon data from the Sonsela Sandstone bed near the Sonsela Buttes, northeastern Arizona, USA, support the presence of a distributive fluvial system: Geosphere, v. 15, p. 1128–1139, https://doi.org/10.1130/GES02004.1.

Martinez, R.N., Sereno, P.C., Alcober, O.A., Colombi, C.E., Renne, P.R., Montañez, I.P., and Currie, B.S., 2011, A basal dinosaur from the dawn of the dinosaur era in southwestern Pangaea: Science, v. 331, p. 206–210, https://doi.org/10.1126/science.1198467.

Martz, J.W., and Parker, W.G., 2010, Revised lithostratigraphy of the Sonsela Member (Chinle Formation, Upper Triassic) in the southern part of Petrified Forest National Park, Arizona: Plos One, v. 5, e9329, p. 1–26, https://doi.org/10.1371/journal.pone.0009329.

Martz, J.W., and Parker, W.G., 2017, Revised formulation of the Late Triassic land vertebrate "faunachrons" of western North America: Recommendations for codifying nascent systems of vertebrate biochronology, *in* Zeigler, K.E., and Parker, W.G., eds., Terrestrial Depositional Systems: Deciphering Complexities Through Multiple Stratigraphic Methods: Amsterdam, Elsevier, p. 39–124, https://doi.org/10.1016/B978-0-12-803243-5.00002-9.

Martz, J.W., Raucci, J.J., Skinner, L., Parker, W.G., Blakey, R.C., and Umhoefer, P., 2012, Geologic map of Petrified Forest National Park, Arizona: Arizona Geological Survey Contributed Map CM-12-A, scale 1:50,000, 1 map sheet, 18 p.

Mattinson, J.M., 2005, Zircon U–Pb chemical abrasion ("CA–TIMS") method: Combined annealing and multi-step partial dissolution analysis for improved precision and accuracy of zircon ages: Chemical Geology, v. 220, p. 47–66, https://doi.org/10.1016/j.chemgeo.2005.03.011.

Mattinson, J.M., 2010, Analysis of the relative decay constants of ^{235}U and ^{238}U by multi-step CA–TIMS measurements of closed-system natural zircon samples: Chemical Geology, v. 275, p. 186–198, https://doi.org/10.1016/j.chemgeo.2010.05.007.

McLean, N.M., Bowring, J.F., Bowring, S.A. and Schoene, R.B., 2008, More than just an age: quantitative analysis of geochronological data and uncertainty: In 2008 Joint Meeting of The Geological Society of America, Soil Science Society of America, American Society of Agronomy, Crop Science Society of America, Gulf Coast Association of Geological Societies with the Gulf Coast Section of SEPM.

Miller, D.S., and Kulp, J.L., 1958, Isotopic study of some Colorado Plateau ores: Economic Geology, v. 53, p. 937–948, https://doi.org/10.2113/gsecongeo.53.8.937.

Miller, D.S., and Kulp, J.L., 1963, Isotopic evidence on the origin of the Colorado Plateau uranium ores: Geological Society of America Bulletin, v. 74, p. 609–630, https://doi.org/10.1130/0016-7606(1963)74[609:IEOTOO]2.0.CO;2.

Morales, M., 1987, Terrestrial fauna and flora from the Triassic Moenkopi Formation of the southwestern United States: Journal of the Arizona–Nevada Academy of Science, v. 22, p. 1–19.

Mundil, R., 2007, Critical view of the calibration of the Triassic time scale: New Mexico Museum of Natural History and Science Bulletin, v. 41, p. 314–315.

Mundil, R., and Irmis, R.B., 2008, New U-Pb age constraints for terrestrial sediments in the Late Triassic: Implications for faunal evolution and correlations with marine environments: 33rd International Geological Congress Meeting, Oslo, abstract HPF-16.

Mundil, R., Ludwig, K.R., Metcalfe, I., and Renne, P.R., 2004, Age and timing of the Permian mass extinctions: U/Pb dating of closed-system zircons: Science, v. 305, p. 1760–1763, https://doi.org/10.1126/science.1101012.

Mundil, R., Pálfy, J., Renne, P.R., and Brack, P., 2010, The Triassic timescale: New constraints and a review of geochronological data, *in* Lucas, S.G., ed., The Triassic Timescale: Geological Society, London, Special Publication 334, p. 41–60, https://doi.org/10.1144/SP334.3.

Nesbitt, S.J., Irmis, R.B., and Parker, W.G., 2007, A critical re-evaluation of the Late Triassic dinosaur taxa of North America: Journal of Systematic Palaeontology, v. 5, p. 209–243, https://doi.org/10.1017/S1477201907002040.

Nordt, L., Atchley, S., and Dworkin, S., 2015, Collapse of the Late Triassic megamonsoon in western equatorial Pangea, present-day American Southwest: Geological Society of America Bulletin, v. 127, p. 1798–1815, https://doi.org/10.1130/B31186.1.

Ogg, J.G., 2012, Triassic, *in* Gradstein, F.M., Ogg, J.G., Schmitz, M.D., and Ogg, G.M., eds., The Geologic Time Scale 2012: Amsterdam, Elsevier, p. 681–730, https://doi.org/10.1016/B978-0-444-59425-9.00025-1.

Olsen, P.E., 1997, Stratigraphic record of the early Mesozoic breakup of Pangea in the Laurasia–Gondwana rift system: Annual Review of Earth and Planetary Sciences, v. 25, p. 337–401, https://doi.org/10.1146/annurev.earth.25.1.337.

Olsen, P.E., and Huber, P., 1998, The oldest Late Triassic footprint assemblage from North America (Pekin Formation, Deep River Basin, North Carolina, USA): Southeastern Geology, v. 38, p. 77–90.

Olsen, P.E., and Kent, D.V., 2000, High-resolution early Mesozoic Pangean climatic transect in lacustrine environments: Zentralblatt für Geologie und Paläontologie, Teil 1, v. 8, p. 1475–1495.

Olsen, P.E., Kent, D.V., Sues, H.-D., Koeberl, C., Huber, H., Montanari, A., Rainforth, E.C., Fowell, S.J., Szajna, M.J., and Hartline, B.W., 2002, Ascent of dinosaurs linked to an iridium anomaly at the Triassic–Jurassic boundary: Science, v. 296, p. 1305–1307, https://doi.org/10.1126/science.1065522.

Olsen, P.E., Kent, D.V., and Whiteside, J.H., 2010, Implications of the Newark Supergroup-based astrochronology and geomagnetic polarity time scale (Newark-APTS) for the tempo and mode of the early diversification of the Dinosauria: Earth and Environmental Science Transactions of the Royal Society of Edinburgh, v. 101, p. 201–229, https://doi.org/10.1017/S1755691011020032.

Olsen, P.E., Reid, J.C., Taylor, K.B., Whiteside, J.H., and Kent, D.V., 2015, Revised stratigraphy of Late Triassic age strata of the Dan River Basin (Virginia and North Carolina, USA) based on drill core and outcrop data: Southeastern Geology, v. 15, p. 1–31.

Olsen, P.E., Geissman, J.W., Kent, D.V., Gehrels, G.E., Mundil, R., Irmis, R.B., Lepre, C., Rasmussen, C., Giesler, D., Parker, W.G., Zakharova, N., Kürschner, W.M., Miller, C., Baranyi, V., Schaller, M.F., Whiteside, J.H., Schnurrenberger, D., Noren, A., Brady Shannon, K., O'Grady, R., Colbert, M.W., Maisano, J., Edey, D., Kinney, S.T., Molina-Garza, R., Bachman, G.H., Sha, J., and the CPCD team: Colorado Plateau Coring Project, 2018, Phase I (CPCP-I): A continuously cored, globally exportable chronology of Triassic continental environmental change from western North America: Scientific Drilling, v. 24, p. 15–40, https://doi.org/10.5194/sd-24-15-2018.

Olsen, P.E., Laskar, J., Kent, D.V., Kinney, S.T., Reynolds, D.J., Sha, J., and Whiteside, J.H., 2019, Mapping Solar System chaos with the Geological Orrery: Proceedings of the National Academy of Sciences of the United States of America, v. 116, p. 10664–10673, https://doi.org/10.1073/pnas.1813901116.

Parker, W.G., 2005, A new species of the Late Triassic aetosaur *Desmatosuchus* (Archosauria: Pseudosuchia): Comptes Rendus Palévol, v. 4, p. 327–340, https://doi.org/10.1016/j.crpv.2005.03.002.

Parker, W.G., 2006, The stratigraphic distribution of major fossil localities in Petrified Forest National Park, Arizona: Museum of Northern Arizona Bulletin, v. 62, p. 46–61.

Parker, W.G., 2018, Redescription of *Calyptosuchus* (*Stagonolepis*) *wellesi* (Archosauria: Pseudosuchia: Aetosauria) from the Late Triassic of the southwestern United States with a discussion of genera in vertebrate paleontology: PeerJ, v. 6, p. e4291, https://doi.org/10.7717/peerj.4291.

Parker, W.G., and Martz, J.W., 2010, The Late Triassic (Norian) Adamanian–Revueltian tetrapod faunal transition in the Chinle Formation of Petrified Forest National Park, Arizona: Earth and Environmental Science Transactions of the Royal Society of Edinburgh, v. 101, p. 231–260, https://doi.org/10.1017/S1755691011020020.

Parker, W.G., and Martz, J.W., 2017, Building local biostratigraphic models for the Upper Triassic of western North America: Methods and considerations, *in* Zeigler, K.E., and Parker, W.G., eds., Terrestrial Depositional Systems: Deciphering Complexities Through Multiple Stratigraphic Methods: Amsterdam, Elsevier, p. 1–38, https://doi.org/10.1016/B978-0-12-803243-5.00001-7.

Payne, J.L., Lehrmann, D.J., Wei, J., Orchard, M.J., Schrag, D.P., and Knoll, A.H., 2004, Large perturbations of the carbon cycle during recovery from the end-Permian extinction: Science, v. 305, p. 506–509, https://doi.org/10.1126/science.1097023.

Peirce, H.W., Shafiqullah, M., and Breed, W.J., 1985, Geochronology of some exotic cobbles, Chinle Formation, Arizona, Abstracts of the Symposium on Southwest Geology: Flagstaff, Museum of Northern Arizona, p. 7.

Peyer, K., Carter, J.G., Sues, H.-D., Novak, S.E., and Olsen, P.E., 2008, A new suchian archosaur from the Upper Triassic of North Carolina: Journal of Vertebrate Paleontology, v. 28, p. 363–381, https://doi.org/10.1671/0272-4634(2008)28[363:ANSAFT]2.0.CO;2.

Pipiringos, G.N., and O'Sullivan, R.B., 1978, Principal unconformities in Triassic and Jurassic rocks, Western Interior United States—A preliminary survey: U.S. Geological Survey Professional Paper 1035-A, p. A1–A29, https://doi.org/10.3133/pp1035A.

Preto, N., Kustatscher, E., and Wignall, P.B., 2010, Triassic climates—State of the art and perspectives: Palaeogeography, Palaeoclimatology, Palaeoecology, v. 290, p. 1–10, https://doi.org/10.1016/j.palaeo.2010.03.015.

Pullen, A., Ibáñez-Mejia, M., Gehrels, G.E., Giesler, D., and Pecha, M., 2018, Optimization of a laser ablation–single collector–inductively coupled plasma–mass spectrometer (Thermo Element 2) for accurate, precise, and efficient Zircon U-Th-Pb geochronology: Geochemistry, Geophysics, Geosystems, v. 19, p. 3689–3705, https://doi.org/10.1029/2018GC007889.

Ramezani, J., Bowring, S.A., Pringle, M.S., Winslow, F.D., III, and Rasbury, E.T., 2005, The Manicouagan impact melt rock: a proposed standard for the intercalibration of U–Pb and ^{40}Ar/^{39}Ar isotopic systems: Moscow, Idahow, 15th V.M. Goldsmidt Conference Abstract Volume, p. A321.

Ramezani, J., Hoke, G.D., Fastovsky, D.E., Bowring, S.A., Therrien, F., Dworkin, S.I., Atchley, S.C., and Nordt, L.C., 2011, High-precision U-Pb zircon geochronology of the Late Triassic Chinle Formation, Petrified Forest National Park (Arizona, USA): Temporal constraints on the early evolution of dinosaurs: Geological Society of America Bulletin, v. 123, p. 2142–2159, https://doi.org/10.1130/B30433.1.

Ramezani, J., Fastovsky, D.E., and Bowring, S.A., 2014, Revised chronostratigraphy of the lower Chinle Formation strata in Arizona and New Mexico (USA): High-precision U-Pb geochronological constraints on the Late Triassic evolution of dinosaurs: American Journal of Science, v. 314, p. 981–1008, https://doi.org/10.2475/06.2014.01.

Rehkämper, M., Schönbächler, M., and Stirling, C.H., 2001, Multiple collector ICP-MS: Introduction to instrumentation, measurement techniques and analytical capabilities: Geostandards Newsletter, v. 25, p. 23–40, https://doi.org/10.1111/j.1751-908X.2001.tb00785.x.

Reichgelt, T., Parker, W.G., Martz, J.W., Conran, J.G., van Konijnenburg-van Cittert, J.H., and Kürschner, W.M., 2013, The palynology of the Sonsela Member (Late Triassic, Norian) at Petrified Forest National Park, Arizona, USA: Review of Palaeobotany and Palynology, v. 189, p. 18–28, https://doi.org/10.1016/j.revpalbo.2012.11.001.

Riggs, N.R., Lehman, T.M., Gehrels, G.E., and Dickinson, W.R., 1996, Detrital zircon link between headwaters and terminus of the Upper Triassic Chinle–Dockum paleoriver system: Science, v. 273, p. 97–100, https://doi.org/10.1126/science.273.5271.97.

Riggs, N.R., Ash, S.R., Barth, A.P., Gehrels, G.E., and Wooden, J.L., 2003, Isotopic age of the Black Forest Bed, Petrified Forest Member, Chinle Formation, Arizona: An example of dating a continental sandstone: Geological Society of America Bulletin, v. 115, p. 1315–1323, https://doi.org/10.1130/B25254.1.

Riggs, N.R., Barth, A.P., González-León, C.M., Jacobson, C.E., Wooden, J.L., Howell, E.R., and Walker, J.D., 2012, Provenance of Upper Triassic strata in southwestern North America as suggested by isotopic analysis and chemistry of zircon crystals: Mineralogical and geochemical approaches to provenance, *in* Rasbury, E.T., Hemming, S.R., and Riggs, N.R., Mineralogical and Geochemical Approaches to Provenance: Geological Society of America Special Paper 487, p. 13–36, https://doi.org/10.1130/2012.2487(02).

Riggs, N.R., Reynolds, S.J., Lindner, P.J., Howell, E.R., Barth, A.P., Parker, W.G., and Walker, J.D., 2013, The Early Mesozoic Cordilleran arc and Late Triassic paleotopography: The detrital record in Upper Triassic sedimentary successions on and off the Colorado Plateau: Geosphere, v. 9, p. 602–613, https://doi.org/10.1130/GES00860.1.

Riggs, N.R., Oberling, Z.A., Howell, E.R., Parker, W.G., Barth, A.P., Cecil, M.R., and Martz, J.W., 2016, Sources of volcanic detritus in the basal Chinle Formation, southwestern Laurentia, and implications for the Early Mesozoic magmatic arc: Geosphere, v. 12, p. 439–463, https://doi.org/10.1130/GES01238.1.

Robertson, W.A., 1967, Manicouagan, Quebec, paleomagnetic results: Canadian Journal of Earth Sciences, v. 4, p. 641–649, https://doi.org/10.1139/e67-041.

Robinson, P.L., 1973, Palaeoclimatology and continental drift, *in* Tarling, D.H., and Runcorn, S.K., eds., Implications of Continental Drift to the Earth Sciences, Volume 1: London, Academic Press, p. 451–476.

Rogers, R.R., 1997, Ischigualasto Formation, *in* Currie, P.J., and Padian, K., eds., Encyclopedia of Dinosaurs: San Diego, California, Academic Press, p. 372–374.

Rogers, R.R., Swisher, C.C., III, Sereno, P.C., Monetta, A.M., Forster, C.A., and Martínez, R.N., 1993, The Ischigualasto tetrapod assemblage (Late Triassic, Argentina) and ^{40}Ar/^{39}Ar dating of dinosaur origins: Science, v. 260, p. 794–797, https://doi.org/10.1126/science.260.5109.794.

Russ, G.P., and Bazan, J., 1987, Isotopic ratio measurements with an inductively coupled plasma source mass spectrometer: Spectrochimica Acta. Part B: Atomic Spectroscopy, v. 42, p. 49–62, https://doi.org/10.1016/0584-8547(87)80049-6.

Schaller, M.F., Wright, J.D., and Kent, D.V., 2015, A 30 Myr record of Late Triassic atmospheric pCO_2 variation reflects a fundamental control of the carbon cycle by changes in continental weathering: Geological Society of America Bulletin, v. 127, p. 661–671, https://doi.org/10.1130/B31107.1.

Schaltegger, U., Guex, J., Bartolini, A., Schoene, B., and Ovtcharova, M., 2008, Precise U-Pb age constraints for end-Triassic mass extinction, its correlation to volcanism and Hettangian post-extinction recovery: Earth and Planetary Science Letters, v. 267, p. 266–275, https://doi.org/10.1016/j.epsl.2007.11.031.

Schmieder, M., Buchner, E., Schwarz, W.H., Trieloff, M., and Lambert, P., 2010, A Rhaetian ^{40}Ar/^{39}Ar age for the Rochechouart impact structure (France) and implications for the latest Triassic sedimentary record: Meteoritics & Planetary Science, v. 45, p. 1225–1242, https://doi.org/10.1111/j.1945-5100.2010.01070.x.

Schmieder, M., Jourdan, F., Tohver, E., and Cloutis, E.A., 2014, ^{40}Ar/^{39}Ar age of the Lake Saint Martin impact structure (Canada)—Unchaining the Late Triassic terrestrial impact craters: Earth and Planetary Science Letters, v. 406, p. 37–48, https://doi.org/10.1016/j.epsl.2014.08.037.

Schoene, B., Crowley, J.L., Condon, D.J., Schmitz, M.D., and Bowring, S.A., 2006, Reassessing the uranium decay constants for geochronology using ID–TIMS U–Pb data: Geochimica et Cosmochimica Acta, v. 70, p. 426–445, https://doi.org/10.1016/j.gca.2005.09.007.

Schoene, B., Guex, J., Bartolini, A., Schaltegger, U., and Blackburn, T.J., 2010, Correlating the end-Triassic mass extinction and flood basalt volcanism at the 100 ka level: Geology, v. 38, p. 387–390, https://doi.org/10.1130/G30683.1.

Scholz, D., and Hoffmann, D.L., 2011, StalAge—An algorithm designed for construction of speleothem age models: Quaternary Geochronology, v. 6, p. 369–382, https://doi.org/10.1016/j.quageo.2011.02.002.

Schultz, L.G., 1963, Clay minerals in Triassic rocks of the Colorado Plateau: U.S. Geological Survey Bulletin, v. 1147-C, p. C1–C71.

Shipman, T.C., 2004, Links between sediment accumulation rates and the development of alluvial architecture; Triassic Ischigualasto Formation, northwestern Argentina [Ph.D. thesis]: Tucson, University of Arizona, 187 p.

Stanley, G.D., Jr., 2003, The evolution of modern corals and their early history: Earth-Science Reviews, v. 60, p. 195–225, https://doi.org/10.1016/S0012-8252(02)00104-6.

Steiner, M.B., Morales, M., and Shoemaker, E.M., 1993, Magnetostratigraphic, biostratigraphic, and lithologic

correlations in Triassic strata of the western United States, *in* Aïssaoui, D.M., McNeill, D.F., and Hurley, N.F., eds., Applications of Paleomagnetism to Sedimentary Geology: SEPM (Society for Sedimentary Geology) Special Publication, v. 49, p. 41–57, https://doi.org/10.2110/pec.93.49.0041.

Stocker, M.R., Nesbitt, S.J., Kligman, B.T., Paluh, D.J., Marsh, A.D., Blackburn, D.C., and Parker, W.G., 2019, The earliest equatorial record of frogs from the Late Triassic of Arizona: Biology Letters, v. 15, no. 2, p. 1–5, https://doi.org/10.1098/rsbl.2018.0922.

Storck, J.-C., Brack, P., Wotzlaw, J.-F., and Ulmer, P., 2019, Timing and evolution of Middle Triassic magmatism in the southern Alps (northern Italy): Journal of the Geological Society, v. 176, p. 253–268, https://doi.org/10.1144/jgs2018-123.

Stewart, J.H., Poole, F.G., and Wilson, R.F., 1972a, Stratigraphy and origin of the Chinle Formation and related Upper Triassic strata in the Colorado Plateau region: U.S. Geological Survey Professional Paper 690, p. 1–336, https://doi.org/10.3133/pp690.

Stewart, J.H., Poole, F.G., Wilson, R.F., and Cadigan, R.A., 1972b, Stratigraphy and origin of the Triassic Moenkopi Formation and related strata in the Colorado Plateau region: U.S. Geological Survey Professional Paper 691, p. 1–195.

Stewart, J.H., Anderson, T.H., Haxel, G.B., Silver, L.T., and Wright, J.E., 1986, Late Triassic paleogeography of the southern Cordillera: The problem of a source for voluminous volcanic detritus in the Chinle Formation of the Colorado Plateau region: Geology, v. 14, p. 567–570, https://doi.org/10.1130/0091-7613(1986)14<567:LTPOTS>2.0.CO;2.

Sues, H.-D., and Olsen, P.E., 2015, Stratigraphic and temporal context and faunal diversity of Permian–Jurassic continental tetrapod assemblages from the Fundy rift basin, eastern Canada: Atlantic Geology, v. 51, p. 139–205, https://doi.org/10.4138/atlgeol.2015.006.

Sues, H.-D., Olsen, P.E., Carter, J.G., and Scott, D.M., 2003, A new crocodylomorph archosaur from the Upper Triassic of North Carolina: Journal of Vertebrate Paleontology, v. 23, p. 329–343, https://doi.org/10.1671/0272-4634(2003)023[0329:ANCAFT]2.0.CO;2.

Trendell, A.M., Atchley, S.C., and Nordt, L.C., 2012, Depositional and diagenetic controls on reservoir attributes within a fluvial outcrop analog: Upper Triassic Sonsela Member of the Chinle Formation, Petrified Forest National Park, Arizona: The American Association of Petroleum Geologists Bulletin, v. 96, no. 4, p. 679–707, https://doi.org/10.1306/08101111025.

Trendell, A.M., Atchley, S.C., and Nordt, L.C., 2013, Facies analysis of a probable large-fluvial-fan depositional system: The Upper Triassic Chinle Formation at Petrified Forest National Park, Arizona, U.S.A: Journal of Sedimentary Research, v. 83, p. 873–895, https://doi.org/10.2110/jsr.2013.55.

Trujillo, K.C., Foster, J.R., Hunt-Foster, R.K., and Chamberlain, K.R., 2014, A U/Pb age for the Mygatt–Moore Quarry, Upper Jurassic Morrison Formation, Mesa County, Colorado: Volumina Jurassica, v. 12, no. 2, p. 107–114.

Walker, J.D., Geissman, J.W., Bowring, S.A., and Babcock, L.E., compilers, 2018, Geologic Time Scale v. 5.0: Boulder, Colorado, Geological Society of America, https://doi.org/10.1130/2018.CTS005R3C.

Whiteside, J.H., Olsen, P.E., Eglinton, T., Brookfield, M.E., and Sambrotto, R.N., 2010, Compound-specific carbon isotopes from Earth's largest flood basalt eruptions directly linked to the end-Triassic mass extinction: Proceedings of the National Academy of Sciences of the United States of America, v. 107, p. 6721–6725, https://doi.org/10.1073/pnas.1001706107.

Whiteside, J.H., Grogan, D.S., Olsen, P.E., and Kent, D.V., 2011, Climatically driven biogeographic provinces of Late Triassic tropical Pangea: Proceedings of the National Academy of Sciences of the United States of America, v. 108, p. 8972–8977, https://doi.org/10.1073/pnas.1102473108.

Whiteside, J.W., Lindström, S., Irmis, R.B., Glasspool, I.J., Schaller, M.F., Dunlavey, M., Nesbitt, S.J., Smith, N.D., and Turner, A.H., 2015, Extreme ecosystem instability suppressed tropical dinosaur dominance for 30 million years: Proceedings of the National Academy of Sciences of the United States of America, v. 112, p. 7909–7913, https://doi.org/10.1073/pnas.1505252112.

Woody, D.T., 2006, Revised stratigraphy of the lower Chinle Formation (Upper Triassic) of Petrified Forest National Park, Arizona: Museum of Northern Arizona Bulletin, v. 62, p. 17–45.

Wotzlaw, J.-F., Guex, J., Bartolini, A., Gallet, Y., Krystyn, L., McRoberts, C.A., Taylor, D., Schoene, B., and Schaltegger, U., 2014, Towards accurate numerical calibration of the Late Triassic: High-precision U-Pb geochronology constraints on the duration of the Rhaetian: Geology, v. 42, no. 7, p. 571–574, https://doi.org/10.1130/G35612.1.

Wotzlaw, J.F., Brack, P., and Storck, J.C., 2018, High-resolution stratigraphy and zircon U–Pb geochronology of the Middle Triassic Buchenstein Formation (Dolomites, northern Italy): Precession-forcing of hemipelagic carbonate sedimentation and calibration of the Anisian–Ladinian boundary interval: Journal of the Geological Society, v. 175, p. 71–85, https://doi.org/10.1144/jgs2017-052.

Zanno, L.E., Drymala, S., Nesbitt, S.J., and Schneider, V.P., 2015, Early crocodylomorph increases top tier predator diversity during rise of dinosaurs: Scientific Reports, v. 5, no. 9276, https://doi.org/10.1038/srep09276.

Zeigler, K.E., Parker, W.G., and Martz, J.W., 2017, The lower Chinle Formation (Late Triassic) at Petrified Forest National Park, southwestern USA: A case study in magnetostratigraphic correlation, *in* Zeigler, K.E., and Parker, W.G., eds., Terrestrial Depositional Systems: Deciphering Complexities Through Multiple Stratigraphic Methods: Amsterdam, Elsevier, p. 237–277, https://doi.org/10.1016/B978-0-12-803243-5.00006-6.